UNIVERSIDADE
BEIRA INTERIOR

Development and characterization of nanomaterials containing IR780 for breast cancer combinatorial therapy

Micaela Guimarães Da Nave

Dissertação para obtenção do Grau de Mestre em
Biotecnologia
(2º ciclo de estudos)

Orientador: Professor Doutor Ilídio Joaquim Sobreira Correia
Co-orientador: Doutor Duarte Miguel de Melo Diogo
Co-orientador: Mestre Cátia Gomes Alves

outubro de 2022

Declaração de Integridade

Eu, Micaela Guimarães Da Nave, que abaixo assino, estudante com o número de inscrição M10727 de Biotecnologia da Faculdade de Ciências, declaro ter desenvolvido o presente trabalho e elaborado o presente texto em total consonância com o **Código de Integridades da Universidade da Beira Interior**.

Mais concretamente afirmo não ter incorrido em qualquer das variedades de Fraude Académica, e que aqui declaro conhecer, que em particular atendi à exigida referenciação de frases, extratos, imagens e outras formas de trabalho intelectual, e assumindo assim na íntegra as responsabilidades da autoria.

Universidade da Beira Interior, Covilhã 06/10/2022

“ Le talent, ça n’existe pas.
Le talent, c’est d’avoir envie de faire quelque chose. ”

- Jacques Brel

Acknowledgments

Antes de mais, queria agradecer ao meu orientador Professor Doutor Ilídio Correia, pela oportunidade que me deu e por me ter proporcionado as melhores condições para o desenvolvimento da minha dissertação. Agradeço também pelo conhecimento e conselhos que me transmitiu ao longo deste ano.

Ao meu co-orientador Doutor Duarte Diogo agradeço todos os conselhos, apoio e dedicação que me forneceu. Agradeço a motivação que sempre me conseguiu transmitir quando os dias corriam menos bem, e por sempre me ajudar a encontrar uma solução aos problemas que enfrentámos. Queria também agradecer-lhe por todo o conhecimento que me transmitiu durante este último ano de mestrado.

À minha co-orientadora Mestre Cátia Alves, agradeço por todo o conhecimento que me transmitiu tanto no laboratório como no restante da dissertação e pela ajuda e paciência em todas as minhas dúvidas e questões durante este ano. Obrigada também por todos os conselhos, por todas as boas conversas que tivemos e pela dedicação. Obrigada por tudo!

Também quero agradecer aos meus companheiros de mestrado, Adriana, Francisco e André. Por todos os momentos passados juntos. Adriana, apesar de não te conhecer, tornaste-te uma grande amiga e ajuda durante este ano. Nunca me esquecerei das nossas conversas e desabafos. Ao Francisco, por todos estes anos que nos conhecemos, obrigada pelos conselhos e por todas as vezes que fomos juntos ver as nossas "filhas". André, obrigada por tentares criar sempre um ambiente com mais risos na nossa salinha e pela nossa grande competição de quem lavava mais falcons.

Um grande obrigado aos restantes colegas de laboratório, por me terem aconselhado e ajudado sempre que puderam.

Quero também agradecer à minha família e amigos, por todo o apoio que me têm dado sobretudo nestes últimos anos que nem sempre foram fáceis. Em primeiro lugar, quero agradecer aos meus pais, por tudo o que fizeram por mim, pelos sacrifícios todos que passaram para termos uma vida melhor. *Je vous aime très fort. Comme pai dit on va arriver à s'en sortir.* Obrigada aos dois por sempre confiarem em mim. Quero também agradecer à minha irmãzinha Flávia que sempre me apoiou nos momentos mais difíceis e que sempre acreditou em mim. Que a nossa cumplicidade se mantenha sempre assim. *Je t'aime*. À minha avó Otília e à *mamie* e ao *papi* obrigada por tudo o que têm feito por mim.

Obrigada por serem os melhores avós. Quero agradecer também à *tata* e ao *tonton* por sempre terem tratado de mim, ao Eric e à Elisabete, à minha tia Branquinha e aos meus padrinhos por me terem ajudado nesta grande etapa. Agora, queria dar um agradecimento especial ao meu namorado Zé. Obrigada por todo o apoio e por todos os momentos que temos vivido juntos. Por todos as visitas, trilhos e passeios que temos feito com o Pacco e o Balu. Obrigada por me teres sempre ajudado, acalmado e aconselhado quando as coisas corriam menos bem. Por fim, queria agradecer também ao Pacco, o meu lindo cão, pela sua felicidade quando chego a casa e por todo o mimo e passeios que damos juntos.

Resumo

Atualmente, de entre os diferentes tipos de cancro, o da mama é o que tem uma maior taxa de mortalidade nas mulheres. Este fenómeno deve-se, em parte, à baixa eficácia e toxicidade não específica dos tratamentos utilizados atualmente em meio clínico (p. ex. cirurgia, quimioterapia, radioterapia). Deste modo, é necessário desenvolver novas abordagens terapêuticas mais eficazes para aplicar no tratamento desta doença.

Com este objetivo em mente, os investigadores têm desenvolvido novos nanomateriais, sendo que os responsivos à luz na zona do infravermelho próximo (em inglês: *Near Infrared* (NIR); 750 – 1000 nm), têm demonstrado propriedades adequadas para uso na terapia quimio-fotodinâmica/fototérmica do cancro. Após interação com luz NIR, estes nanomateriais produzem espécies reativas de oxigénio (Terapia Fotodinâmica) e/ou um aumento de temperatura (Terapia Fototérmica). Estes dois tipos de terapias têm capacidade de danificar as células cancerígenas. Para além disso, também podem despoletar a libertação de fármacos encapsulados nos nanomateriais.

No entanto, o desenvolvimento de nanomateriais específicos para aplicação na terapia quimio-fotodinâmica/fototérmica é um processo muito complexo. De uma forma geral, primeiro é necessário sintetizar nanomateriais com capacidade fototérmica. De seguida, moléculas fotossensibilizadoras e fármacos quimioterapêuticos são encapsulados nestes nanomateriais, e, por vezes, estes podem ainda ser revestidos com polímeros de forma a apresentarem propriedades biológicas adequadas.

Na presente dissertação de Mestrado, procedeu-se ao desenvolvimento de uma abordagem inovadora e direta para obtenção de nano-sistemas responsivos à luz NIR com capacidade para aplicação na terapia quimio-fotodinâmica/fototérmica do cancro da mama. Para tal procedeu-se à conjugação de poli(2-etil-2-oxazolina) ao IR780, o que permitiu a obtenção de um polímero anfifílico capaz de se organizar em nanopartículas com capacidade fotodinâmica/fototérmica, e que, simultaneamente, encapsulam Doxorrubicina (DOX/PEtOx-IR NPs). Os resultados demonstram que as DOX/PEtOx-IR NPs apresentam um tamanho e carga de superfície adequada para aplicações anti-cancerígenas. Comparativamente com o conjugado PEtOx-IR, verificou-se que as DOX/PEtOx-IR NPs apresentam cerca de 2.4-vezes mais absorção na zona do NIR. Após interação com a luz NIR, as DOX/PEtOx-IR NPs produzem espécies reativas de oxigénio bem como uma pequena variação de temperatura que auxilia em cerca de 1.6-vezes na

libertação da DOX. Devido a esta capacidade, nos estudos *in vitro*, a ação combinada das DOX/PEtOx-IR NPs e da luz NIR conseguiu reduzir a viabilidade das células cancerígenas do cancro da mama para apenas 4 %, demonstrando assim o potencial destes nanomateriais para a terapia quimio-fotodinâmica/fototérmica.

Palavras-chave

IR780;Nanomateriais multifuncionais;Nanomateriais responsivos à luz;Poli(2-etil-2-oxazolina);Terapia combinatória tripla;Terapia fotodinâmica.

Resumo Alargado

O cancro continua a ser uma das doenças que apresenta maior mortalidade a nível mundial. Especificamente, o cancro da mama é o que mais afeta as mulheres. As terapias mais utilizadas para o tratamento do cancro da mama são a quimioterapia, radioterapia e cirurgia. Porém, estas terapias apresentam várias desvantagens, como baixa eficácia e toxicidade não específica, conduzindo a efeitos nefastos nos pacientes. Assim, existe uma enorme demanda para o desenvolvimento de novas abordagens terapêuticas para esta doença.

Com este objetivo em mente, investigadores e profissionais clínicos têm-se focado no desenvolvimento e validação de várias estratégias terapêuticas baseadas em nanomateriais. Estas estruturas à nano-escala conseguem, mediante de otimização de diversas propriedades físico-químicas, acumularem-se preferencialmente no local do tumor, podendo contribuir para um efeito terapêutico mais direcionado. Recentemente, vários grupos de investigação demonstraram que os nanomateriais responsivos à luz na zona do infravermelho próximo (em inglês: *Near Infrared* (NIR); 750 – 1000 nm) têm um potencial acrescido no tratamento do cancro. Estas nanoestruturas, após interagirem com luz NIR, produzem espécies reativas de oxigénio (Terapia Fotodinâmica) e/ou um aumento de temperatura (Terapia Fototérmica), tendo estes efeitos capacidade para danificar as células cancerígenas. Além disso, também podem despoletar a libertação de fármacos encapsulados nos nanomateriais.

Apesar do potencial dos nanomateriais para a terapia quimio-fotodinâmica/fototérmica do cancro, a translação dos mesmos ainda não foi alcançada devido à sua complexa e trabalhosa produção. De uma forma geral, primeiro é necessário sintetizar nanomateriais com capacidade fototérmica. De seguida, moléculas fotossensibilizadoras e fármacos quimioterapêuticos são encapsulados nestes nanomateriais, e, por vezes, estes podem ainda ser revestidos com polímeros de forma a apresentarem propriedades biológicas adequadas.

No trabalho de investigação desta Dissertação de Mestrado, procedeu-se ao desenvolvimento de uma abordagem inovadora e direta para obtenção de nano-sistemas responsivos à luz NIR com capacidade para aplicação na terapia quimio-fotodinâmica/fototérmica do cancro da mama. Para tal finalidade, a poli(2-etil-2-oxazolina) foi conjugada com o IR780, o que permitiu a obtenção de um polímero anfifílico capaz de se organizar em nanopartículas com capacidade

fotodinâmica/fototérmica e que simultaneamente, encapsulam Doxorrubicina (DOX/PEtOx-IR NPs). Os resultados obtidos indicaram que as DOX/PEtOx-IR NPs apresentaram um tamanho (160.7 ± 3.6 nm) e carga superficial (- 9.1 ± 0.3 mV) adequadas para aplicações anticancerígenas. Este nano-sistema revelou ainda uma elevada eficácia de encapsulação, tendo conseguido incorporar aproximadamente 63 ± 4 % de DOX. Comparativamente com o conjugado PEtOx-IR, verificou-se que as DOX/PEtOx-IR NPs apresentam cerca de 2.4-vezes mais absorção na zona do NIR. Este resultado demonstra o potencial fotodinâmico e fototérmico deste nano-sistema. Deste modo, após interação com a luz NIR, as DOX/PEtOx-IR NPs produziram espécies reativas de oxigénio bem como uma pequena variação de temperatura, que auxiliou em cerca de 1.6 vezes a libertação da DOX. Por fim, foram realizados estudos *in vitro* que demonstraram a boa citocompatibilidade das PEtOx-IR NPs (nanoestruturas controlo sem DOX), tanto em células saudáveis como em células do cancro da mama. Por outro lado, a combinação das PEtOx-IR NPs com luz NIR (terapia fotodinâmica/fototérmica mediada por nanomateriais) e as DOX/PEtOx-IR NPs (quimioterapia mediada por nanomateriais) reduziram a viabilidade das células cancerígenas do cancro da mama para 21 e 17 %, respetivamente. Em contraste, a ação combinada das DOX/PEtOx-IR NPs com a luz NIR conduziu à eliminação praticamente total das células do cancro da mama (viabilidade < 4 %), enfatizando o potencial destes nanomateriais para terapia quimio-fotodinâmica/fototérmica.

Abstract

Among the different types of cancer, breast cancer is the one that presents the highest mortality rate among women. This scenario occurs in part due to the low efficacy and non-specific toxicity of the treatments currently available in the clinic (*e.g.* surgery, chemotherapy, radiotherapy). In this way, it is crucial to develop novel therapeutic strategies to tackle this disease.

Nowadays, researchers have been focused on the development of new nanomaterials for cancer therapy. Among them, those responsive to near infrared light (NIR; 750 – 1000 nm) have been explored for combinatorial chemo-photodynamic/photothermal therapy (chemo-PDT/PTT). Upon interaction with this radiation, these nanomaterials produce reactive oxygen species (PDT) and/or promote a temperature increase (PTT). These events can damage cancer cells as well as trigger the release of drugs from nanomaterials' core.

However, the production of nanomaterials aimed for chemo-PDT/PTT is a complex process. Generally, first, nanomaterials with photothermal capacity are synthesized, being then loaded with photosensitizers plus chemotherapeutics and, finally functionalized with polymers for achieving suitable biological properties.

In this Master dissertation, a novel and straightforward approach to attain the production of NIR light-responsive nanosystems for cancer chemo-PDT/PTT was established. Such was accomplished by conjugating poly(2-ethyl-2-oxazoline) to IR780, forming an amphiphilic polymer that can be assembled into nanoparticles with photodynamic/photothermal capabilities, that simultaneously encapsulate Doxorubicin (DOX/PEtOx-IR NPs). The obtained results revealed that the DOX/PEtOx-IR NPs present a suitable size distribution and surface charge for cancer related applications. Compared to the PEtOx-IR conjugate, the DOX/PEtOx-IR NPs showed a 2.4-fold higher NIR absorption. Upon interaction with this radiation, the DOX/PEtOx-IR NPs produced singlet oxygen as well as a small thermic effect that boosted the release of DOX by up to 1.6-times. Owing to this capacity, in the *in vitro* studies, the combination of DOX/PEtOx-IR NPs and NIR light could completely ablate breast cancer cells (viability < 4 %), demonstrating the enhanced outcome arising from the nanomaterials' chemo-photodynamic/photothermal therapy.

Keywords

Combinatorial triple therapy, IR780, Light responsive nanoparticles, Multifunctional nanomaterials, Photodynamic therapy, Poly(2-ethyl-2-oxazoline).

List of Publications

Articles submitted for publication in international peer reviewed journals:

Micaela Nave, Francisco J. P. Costa, Cátia G. Alves, Rita Lima-Sousa, Bruna L. Melo, Ilídio J. Correia, Duarte de Melo-Diogo. Simple preparation of POxylated nanomaterials for cancer chemo-PDT/PTT. *Submitted for publication*.

Francisco J. P. Costa, Micaela Nave, Rita Lima-Sousa, Cátia G. Alves, Bruna L. Melo, Ilídio J. Correia, Duarte de Melo-Diogo. Development of Thiol-Maleimide hydrogels incorporating graphene-bases nanomaterials for cancer chemo-photothermal therapy. *Submitted for publication*.

Rita Lima-Sousa, Cátia G. Alves, Bruna L. Melo, Francisco J. P. Costa, Micaela Nave, André F. Moreira, António G. Mendonça, Ilídio J. Correia, Duarte de Melo-Diogo. Injectable hydrogels for the delivery of nanomaterials aimed for cancer combinatorial photothermal therapy. *Under review*.

Index

Chapter 1

Chapter 2

Chapter 3

Chapter 4

Chapter 5

List of Figures

List of Abbreviations

$^1O_2$	Singlet Oxygen
ANOVA	Analysis of Variance
BRCA1	Breast Cancer Associated Gene 1
BRCA2	Breast Cancer Associated Gene 2
Chemo-PDT/PTT	Chemotherapy combined with Photodynamic/Photothermal Therapy
CLSM	Confocal Laser Scanning Microscopy
DLS	Dynamic Light Scattering
DMEM-F12	Dulbecco's Modified Eagle's Medium-F12
DOX	Doxorubicin
DOX/PEtOx-IR NPs	Doxorubicin loaded Poly(2-ethyl-2-oxazoline)-IR780 Nanoparticles
EPR	Enhanced Permeability and Retention
ER	Estrogen Receptor
ERα	Estrogen Receptor α
FBS	Fetal Bovine Serum
FDA	Food and Drug Administration
FTIR	Fourier Transform Infrared Spectroscopy
HA	Hyaluronic Acid
HER2	Human Epidermal Growth Factor Receptor 2
ICG	Indocyanine Green
K^-	Negative Control
K^+	Positive Control
MCF-7	Michigan Cancer Foundation-7
NHDF	Normal Human Dermal Fibroblasts
NIR	Near-Infrared
NPs	Nanoparticles
n.s.	Non-significant
PBS	Phosphate Buffered Saline
PDI	Polydispersity Index
PDT	Photodynamic Therapy
PEG	Poly(ethylene glycol)
PEtOx	Poly(2-ethyl-2-oxazoline)
PEtOx-IR conjugate	Poly(2-ethyl-2-oxazoline)-IR780 conjugate

PEtOx-IR NPs	Poly(2-ethyl-2-oxazoline)-IR780 Nanoparticles
PEtOx-SH	Poly(2-ethyl-2-oxazoline) α-benzyl ω-thiol terminated
PI	Propidium Iodide
PR	Progesterone Receptor
PTT	Photothermal Therapy
RES	Reticuloendothelial System
ROS	Reactive Oxygen Species
S.D.	Standard Deviation
SOSG	Singlet Oxygen Sensor Green
TNBC	Triple-Negative Breast Cancer
w/ NIR	With NIR laser exposure
w/o NIR	Without NIR laser exposure

Chapter 1

Introduction

1. Introduction

1.1. Cancer

Following heart disease, cancer is the second cause of death in the world, counting with approximately 19.3 million new cases and about 10 million victims in 2020 [1, 2]. In the United States, approximately, 1.9 million new cancer cases and 609 360 cancer deaths are expected to occur in 2022 [3]. This disease seems to have more cases every year, due to the growth of the worldwide population as well as of its aging [1].

According to the World Health Organization, 35 % of cancer deaths can be prevented through lifestyle changes, such as avoiding unhealthy habits [4]. The risk factors can be divided into two different groups: biological and chemical factors (Figure 1) [4]. Tobacco is highlighted as the principal cause of cancer-related deaths [5]. However, an unbalanced diet is also a factor that leads to a higher cancer incidence. It is estimated that 35 % of cancer cases are derived from bad nutrition and lack of physical activities, and 20 % from excessive weight [4, 6].

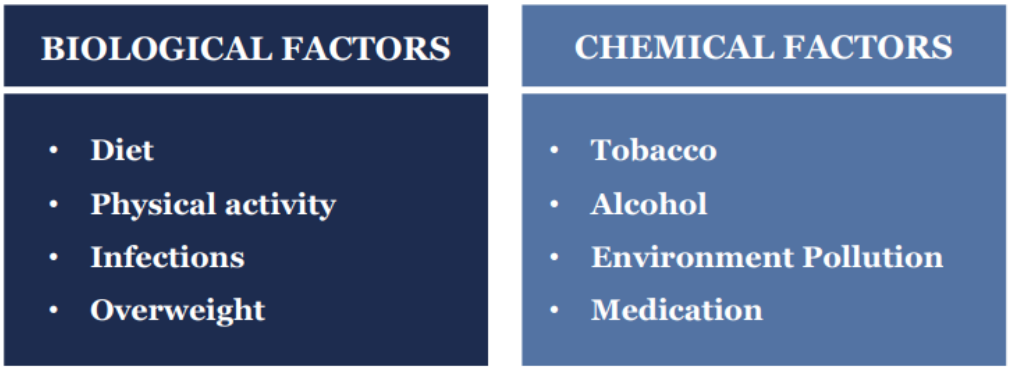

Figure 1. Biological and chemical risk factors that are pointed as the principal causes of cancer.

Cancer can occur as a consequence of genetic and epigenetic modifications, that lead to a state of uncontrolled proliferation of cells [7]. Such appears due to various factors that are reported in the literature [7, 8]. In 2011, Hanahan and Weinberg proposed the following hallmarks of cancer: 1) improved proliferation; 2) growth suppressors invasion; 3) reduction of cellular death; 4) replicative immortality; 5) improved angiogenesis; 6) invasion and metastasis initiation; 7) genome instability and mutations; 8) inflammation; 9) reprogrammed metabolism energy; 10) immune destruction evasion (Figure 2) [8, 9]. More recently, in 2022, Hanahan described four new hallmarks of

cancer: phenotypic plasticity unlocking, non-mutagenic epigenetic reprograming, polymorphic microbiome and senescent cells (Figure 2) [10].

In normal circumstances, the cellular growth and division occur due to the capacity of healthy cells to produce and release growth factors and nutrients, in a controllable fashion [8, 9]. Cancer cells have the ability to overcome the checkpoints of the cell cycle allowing an uncontrolled proliferation [9].

Additionally, the downregulation of the expression of suppressor genes, such as the retinoblastoma-associated protein, LKB1 and cyclin dependent kinase inhibitors, enables cancer cells to create a pathway for a deregulated proliferation [8, 11]. Besides that, anomalies in the transforming growth factor-beta pathway can also result in an uncontrolled proliferation [8, 12].

It is estimated that more than 50 % of cancer cases occur as a consequence of a mutation in the p53 tumor suppressor gene [13]. P53 is a cytoplasmatic protein responsible for genomic stability, metabolic stress, oncogene activation and for the regulation of Bcl-2 protein [14]. Bcl-2 is an anti-apoptotic protein that can have many consequences when its function is altered due to mutations in p53, as this irregularity can lead to diseases, such as cancer [13]. Then, it has been proved that cancer cells can overexpress the Bcl-2 protein and thereby avoid apoptosis [9, 13].

Furthermore, approximately, 85 % of all cancers overexpress telomerase [15]. Telomerase is an enzyme that contributes to chromosome ends' stability, thus when telomerase is highly expressed, cells divide indefinitely, and senescence and apoptosis are avoided, leading to cancer [8, 16].

Additionally, the overexpression of growth factors, such as, vascular endothelial growth factor-A promotes angiogenesis, and have a capability to develop new vessels during embryonic and postnatal process, being these newly formed vessels essential to support tumor's growth [8, 17].

Thus, in addition to being a disease of deregulated cell proliferation, cancer is also a disease of deregulated cell migration [18]. This occurs when metastasis start and cancer cells spread to other body areas, compromising the homeostasis and function of other organs [8, 18].

Microbiome has a deep influence in health and more recently it has been proved their impact in cancer's development, progression and metastasis [10, 19, 20]. Specifically, some

bacteria can directly damage DNA, inducing abnormalities that can trigger cancer's development [10, 20].

In turn, prolonged/chronic inflammatory environments are also associated with a greater presence of nitrogen and oxygen radicals, which can also cause DNA damage and consequently mutations that trigger cancer development [21, 22].

Several factors can cause senescence in cells, including abnormalities in the cellular signaling, organelle and cellular infrastructure damage [10]. Earlier, it was thought that cellular senescence served as a safeguard against neoplasia [10]. Nevertheless, the inverse has been proved [23]. It was demonstrated that senescent cells can promote angiogenesis, invasion and metastasis as well as prevent apoptosis, which in turn stimulates the formation and development of the tumor [10].

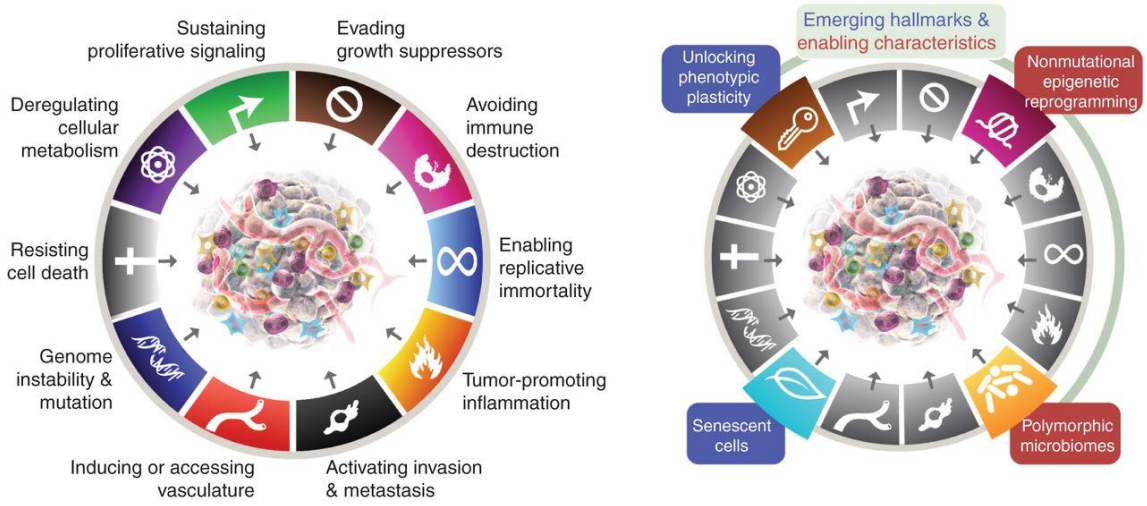

Figure 2. The Hallmarks of Cancer described by Hanahan in 2011 (left) and 2022 (right) (Adapted from [10]).

1.2. Breast Cancer

Breast cancer is the one with the highest incidence in the world and the second deadliest after lung cancer. In women, about 30 % of the diagnosed cases are for breast cancer [2]. In 2020, breast cancer accounted for about 2.2 millions of newly diagnosed cases and approximately 684 000 deaths [2]. In 2022, it is predicted that 51 400 cases of new female breast cancer will be detected in the United States [3]. In Portugal, this scenario is also alarming, with about 7 000 new cases diagnosed in 2020 [24].

Gender is a major risk factor in breast cancer, since this disease has a one hundred times higher incidence in women (the incidence in men is about 1 %). Besides that, male breast cancer has a mortality rate of 0.1 %, while in women it is about 12.5 % [25, 26]. Age is another factor, since there is a higher incidence of breast cancer in women between 40 and 60 years old [25]. Additionally, studies have demonstrated that an unhealthy lifestyle (alcohol consumption, poor physical activity and an unbalanced diet) can contribute to a higher breast cancer risk [4, 25]. Another risk factor is the estrogen levels [25]. There are endogenous (produced in the ovary) and exogenous (oral contraceptives) estrogen, and both contribute to an increased probability of developing breast cancer [25]. Furthermore, women with family members that previously had breast cancer also have a higher probability of developing it [25]. In a study with 113 000 participants, Brewer *et al.* showed that women with close family members with breast cancer were 1.75-times more likely to develop it [27]. There are several genes associated with breast cancer propensity such as human epidermal growth factor receptor 2 (HER2), breast cancer-associated genes 1 and 2 (BRCA-1 and BRCA-2), and hormone receptors, such as estrogen receptor (ER) or progesterone receptor (PR) [25, 28, 29]. The occurrence of mutations in these genes is associated with the development of breast cancer (Figure 3).

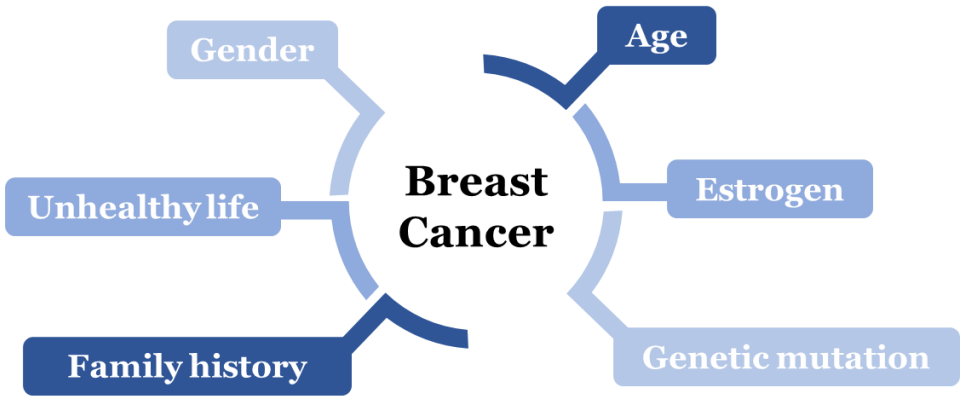

Figure 3. Breast cancer risk factors.

Breast cancer is a heterogeneous disease that starts when epithelial cells proliferate in an uncontrolled way due to carcinogenic factors [25]. Based on the genetic signature, breast cancer can be divided into three types: the one that expresses hormone receptors (positive ER, positive PR, or both), that expresses HER2, and the triple-negative breast cancer (TNBC) [28].

Hormone receptor positive breast cancer represents 75 % of cancer cases [30]. Both estrogen receptor α (ERα) and estrogen receptor β are overexpressed in breast cancer cells

[31, 32]. There is an increased expression of the ERα in breast cancer cells (expression is about 80 % in cancer cells in comparison with 10 % in healthy cells), and thus ER is considered to be responsible for the increased cell proliferation [31, 33]. Progesterone, mainly produced in the ovaries, also leads to unregulated cell proliferation in breast tissue [32].

Approximately 15 – 20 % of breast cancers overexpress HER2, a protein that belongs to the epidermal growth factor family [34]. The overexpression of this protein leads to a deregulated cellular growth and proliferation and to metastatic activity [35].

Finally, triple-negative breast cancer is characterized by the absence of hormone (estrogen and progesterone) and HER2 receptors [36]. This type of cancer represents about 10 – 20 % of breast cancer cases and is more recurrent in younger women [37]. It was demonstrated that TNBC is associated with mutations in BRCA-1 and BRCA-2 genes and about 90 % are invasive ductal carcinomas [37]. The TNBC has a low survival rate due to its aggressiveness and difficulty in its treatment [37].

Nowadays, the most common therapies used for breast cancer treatment are surgery, chemotherapy, and radiotherapy [38]. Surgery is the approach resorted in the early stages of breast cancer and consists in the removal of the tumor [39]. Chemotherapy and radiotherapy aim to kill cancer cells, using drugs and high-energy radiation, respectively [28, 40]. Nevertheless, these therapies, when used individually or simultaneously, have several limitations such as low targeting ability for cancer cells (leading to side effects), and propensity to be affected by resistance mechanisms [41]. Due to these drawbacks, it is of extreme importance the development of new therapeutic approaches to replace the conventional therapeutic strategies for eradicating cancer cells [42].

1.3. Nanomaterials' based Therapies

To overcome the disadvantages of conventional therapies, numerous alternatives have been studied. In particular, in the recent years, nanomaterials-based therapies have been a major focus among researchers [43]. These therapies are characterized by the application of nanomaterials, that can passively accumulate in the tumor area, potentially leading to a greater and more selective therapeutic effect [44].

Over the years, different types of nanomaterials have been developed. Nanostructures such as liposomes, dendrimers, micelles, and polymeric nanoparticles have been widely investigated due to their excellent biocompatibility and biodegradability (Figure 4) [45, 46].

Liposomes are self-assembling nanomaterials based on phospholipids bilayer [45, 47]. With their natural structure, they can encapsulate hydrophobic or hydrophilic agents [45, 48]. In their aqueous core, liposomes can load hydrophilic therapeutic agents, and in the lipidic bilayer, these can encapsulate hydrophobic molecules [44, 45, 48]. Liposomes can protect the loaded cargo from inactivation and degradation in the blood circulation [45, 48]. However, liposomes are rapidly cleared from circulation by the reticuloendothelial system (RES) cells [45, 48].

Buhleier *et al.* and Tomalia *et al.* were the first groups to synthesize nanomaterials with a 3D organized hyperbranched structure, also known as dendrimers [49, 50]. Dendrimers present excellent physical and chemical proprieties, and have high density of functional groups on their surface [45, 49]. The interactions with functional groups enable the easy encapsulation of drugs and genes, and their delivery through the cytoplasmic membrane [50]. Nevertheless, some dendrimers, especially those highly positively charged, can induce some toxicity by causing membrane disruption [50].

In 1980, micelles were described as small spherical self-assembling amphiphilic polymers [45, 51]. Due to their size (5 – 100 nm), they can avoid renal excretion and may display an increased blood circulation time, favoring their tumor uptake [45, 51, 52]. This type of nanomaterial has a hydrophobic core where imaging and/or therapeutic agents can be loaded, and a hydrophilic exterior that ensures micelles' water stability [51, 53]. However, micelles have a reduced stability in physiologic conditions: they can dissociate when the concentration is lower than the critical micelle concentration (this parameter is used to determine the micelles' properties and influences their stability) [52].

Polymeric nanoparticles generally have a large hydrophobic polymeric core, which can then be coated by an hydrophilic shell [54]. Polymeric nanoparticles can encapsulate therapeutic, genetic and imaging agents in their core or shell [45]. Poly(D,L-lactide-*co*-glycolide), poly(ethylene glycol) (PEG), D-α-Tocopherol polyethylene glycol 1000 succinate and polylactic acid are examples of polymers that have been used in the preparation of polymeric nanoparticles [55, 56].

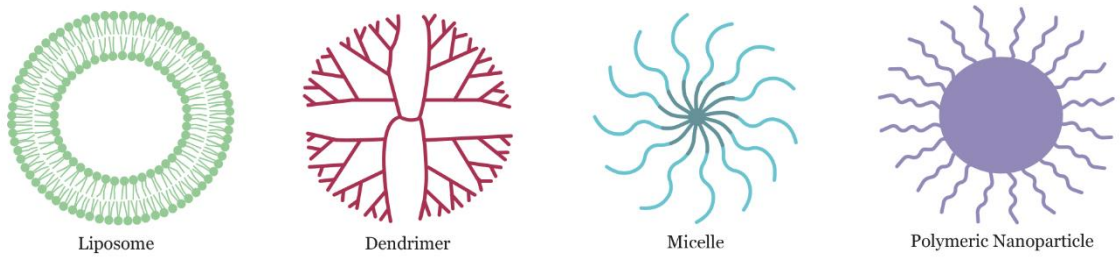

Figure 4. Schematic representation of Liposomes, Dendrimers, Micelles and Polymeric Nanoparticles.

In general, nanomaterials aimed for cancer therapy must display an increased blood circulation time, favoring their accumulation at tumor site, and subsequent penetration and internalization in the cancer cells [57]. To achieve this goal, several nanoparticles' features can be optimized, such as size, charge, corona and targeting decoration [57].

Nanomaterials are usually intravenously injected for reaching the tumor zone. The vessels in the tumor microenvironment display a higher permeability and retention than healthy vessels. This phenomenon is related to the large fenestrae (200 – 1200 nm) that occur in the tumor vessels and due to the impaired lymphatic drainage of the tumor site. This phenomenon is known as the enhanced permeability and retention (EPR) effect [57, 58].

Thus, to attain a maximum accumulation of nanomaterials in the tumor zone, their size is a crucial factor. If the nanomaterial diameter is superior to 200 nm, they will be recognized by macrophages and can become accumulated in the liver and spleen [57-59]. However, if the size is between 3 and 5 nm, the nanomaterials are eliminated by renal filtration [58, 60]. Furthermore, if the diameter is less than 50 nm, the nanomaterial will also become accumulated in the liver [58-60]. Thereby, the ideal size for tumor accumulation is often defined as being between 100 – 200 nm [57, 60, 61].

The circulation time in the bloodstream is also essential to promote nanoparticles' accumulation in the tumor. Nanomaterials with a prolonged blood circulation may have a higher probability to extravasate through the tumor's fenestrae and subsequently reach the tumor. The surface charge of nanoparticles (zeta potential) is another property that influences their blood circulation time and cellular uptake [60]. Nanomaterials with a zeta potential superior to + 10 mV (positively charged) tend to interact with blood components (aggregating) while those with less than - 10 mV (negatively charged) present a greater interaction with RES system cells [58]. In turn, nanostructures with a zeta potential between - 10 mV and + 10 mV (the so-called neutral nanomaterials) tend to be ideal since

these have less interaction with RES system/proteins, leading to a greater blood circulation time and tumor uptake [57, 58].

Another characteristic that influences the time in the bloodstream and the accumulation in the tumor area is the nanomaterial corona [57, 60, 62]. In this way, nanostructures' corona is an important feature that can be modulated to enhance the circulation time, colloidal stability, biodistribution, biocompatibility and cellular accumulation of nanomaterials [57, 58, 60]. The use of hydrophilic polymers, such as PEG and poly(2-ethyl-2-oxazoline) (PEtOx), creates a superficial barrier that protects nanostructures against protein adsorption and improves nanomaterials' properties (biodegradability, biocompatibility and stability) [57, 63, 64]. Coating the nanomaterials with these non-fouling polymers also grant them "invisibility" to the immune system, hence favoring their blood circulation time and tumor uptake [57, 65].

To have a selective internalization in cancer cells, targeting agents have been grafted into the nanomaterials' surface (*e.g.* hyaluronic acid, anti-HER2 antibodies, folic acid) [33, 60, 66, 67]. These targeting agents can further enhance the therapeutic efficiency and reduce the side effects in healthy cells [33, 57].

An alternative strategy to attain a therapeutic effect more selective to the tumor zone relies on the use of nanomaterials' with photodynamic and/or photothermal properties [68, 69]. The onset of these therapies is triggered by external light, and therefore these generally do not induce effects in the non-irradiated areas [70]. In presence of light, nanomaterials with photodynamic properties produce reactive oxygen species (ROS; Photodynamic Therapy (PDT)) [71]. Nanomaterials with photothermal properties can cause a temperature increase upon interaction with light (Photothermal Therapy (PTT)) [42]. Both these stimuli, ROS and temperature increase, can cause damage to cancer cells.

1.4. Nanomaterials' based Phototherapies

Photo-responsive nanomaterials have a great potential for anticancer applications due to their ability to produce a temperature increase and/or reactive oxygen species upon exposure to light. In this context, nanomaterials' phototherapies based on the use of near-infrared (NIR) light (750 – 1000 nm) demonstrate a deep penetration capacity in tissues, presenting minimal interactions with biological components (proteins, collagen, hemoglobin and melanin) – Figure 5 [60, 72, 73]. Therefore, it is essential that

nanomaterials display a high NIR absorption in order to efficiently interact with this radiation.

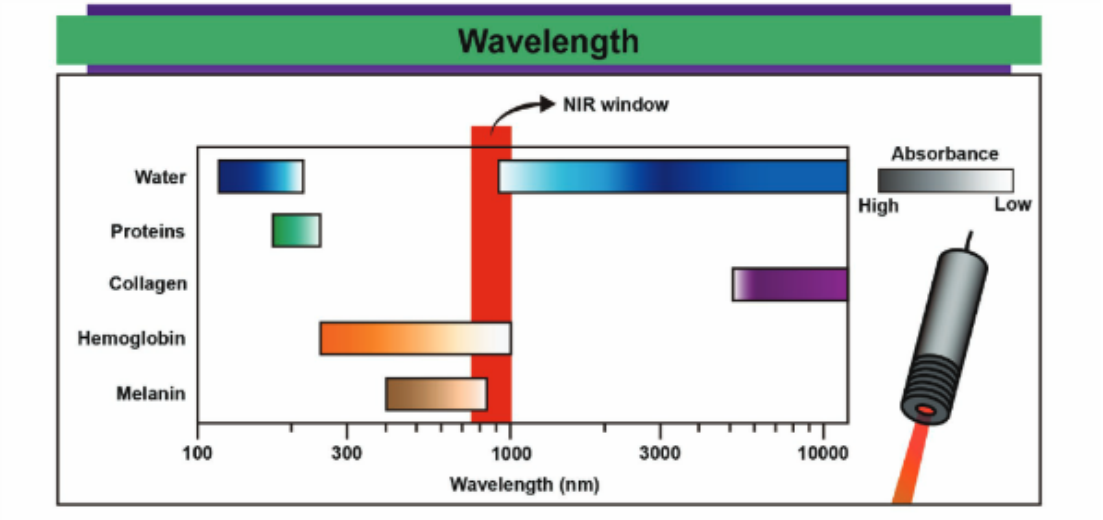

Figure 5. Representation of NIR light interaction with major human body components. Radiation with wavelengths between 750 and 1000 nm (NIR region) has minimal effect on the human body's primary constituents (Adapted from [60]).

After irradiation, photosensitizers produce ROS (*e.g.* singlet oxygen ($^1O_2$), hydrogen peroxide (H_2O_2)) which can oxidate cellular components (*e.g.* proteins, DNA) and consequently induce cell death [70]. In turn, when exposed to NIR light, the photothermal nano-agents absorb its energy, releasing it as heat. Different effects can occur depending on the temperature increase achieved in the tumor area. A hyperthermia at 41.8 °C – 45 °C has been shown to sensitize malignant cells to other therapies, causing a minimal damage in healthy tissues, while final temperatures of 50 °C (or above) can induce irreversible damage (*e.g.* mitochondria and enzymatic dysfunctions), eventually leading to necrosis [60]. Moreover, nanomaterials' mediated PDT/PTT can also be conjugated with other therapeutic modalities in order to attain a synergistic anticancer effect [74].

In the recent years, various NIR light-responsive nanomaterials have been developed, such as graphene oxide, gold nanorods and nanomaterials incorporating NIR-absorbing small molecules [70]. In this regard, researchers have been studying nanomaterials incorporating NIR-absorbing small molecules due to their straightforward preparation and improved biological properties [75, 76]. For instance, Indocyanine green (ICG) loaded nanomaterials have been extensively studied due to the Food and Drug Administration (FDA)-approval status of this NIR dye [46]. However, ICG-loaded nanomaterials present a low photostability and fluorescence quantum yield [77-79]. In this way, ICG alternatives have

been largely studied [79]. Nanomaterials incorporating IR780, a NIR-absorbing prototypic heptamethine cyanine, have been demonstrating promising results for cancer PDT/PTT due to their excellent optical and thermal stability, as well as higher absorption in the NIR region [46]. The preparation of nanomaterials incorporating IR780 is crucial due to the poor water stability, unsuitable cytocompatibility and rapid blood clearance displayed by free IR780 [70, 80].

1.5. Nanomaterials loaded with IR780 for Photodynamic and Photothermal Therapies

The incorporation of IR780 in nanomaterials is crucial to overcome its limitations, hence fully taking advantage of its potential for cancer PDT/PTT. In fact, the incorporation of this NIR dye in nanostructures results in an improved solubility and biocompatibility and also enhances the blood circulation time, tumor accumulation and photodynamic/photothermal capacity (Figure 6) [70].

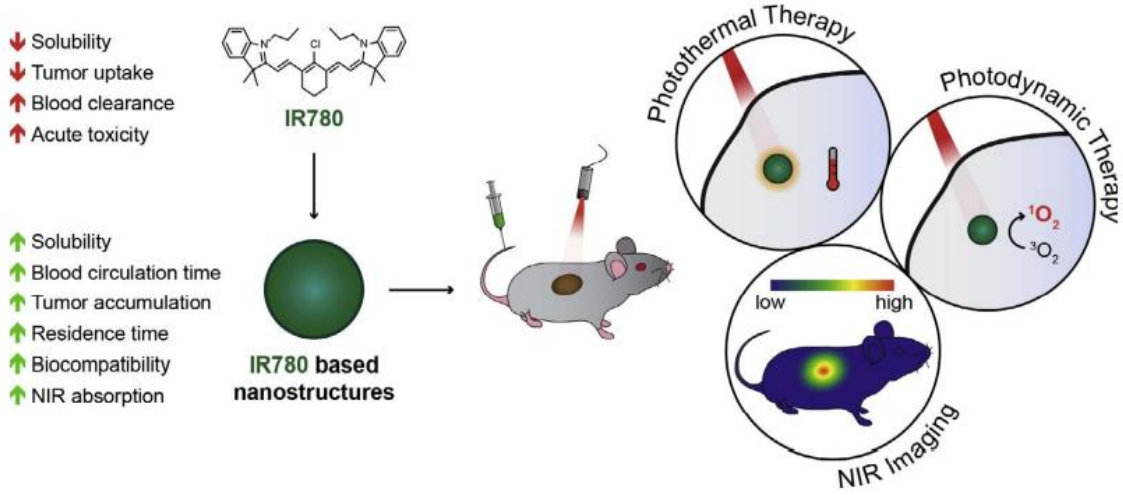

Figure 6. Schematic representation of the advantages of incorporating IR780 in nanostructures (Adapted from [70]).

In general, there are two strategies that can be applied to prepare IR780-nanomaterials: i) the loading of IR780 into the hydrophobic core of PEGylated nanoparticles, and ii) the conjugation of hydrophilic polymers (*e.g.* PEG) to the cyclohexenyl ring of IR780, rendering an amphiphilic polymer that assembles into nanoparticles. The preparation of hydrophilic polymer-IR780 conjugate nanoparticles is a relatively novel approach that improves IR780' solubility and cytocompatibility [81, 82]. In general, when compared with the encapsulation of drugs in the hydrophobic core of the nanomaterials', the polymer-drug conjugate

nanostructures present a straightforward assembly/preparation and a well-regulated drug release [83-85]. These types of polymer-drug conjugate nanostructures also have a high tumor uptake [86]. For instance, Yuan *et al.* produced a PEG-IR780-C13 conjugate that self-assembled into biocompatible micelles with an improved photostability and high tumor uptake [87]. However, several works have proved that the administration of PEGylated nanomaterials can create anti-PEG antibodies [88, 89]. These anti-PEG antibodies mediate the rapid clearance of these nanoparticles in subsequent administrations (the so-called Accelerated Blood Clearance phenomenon). In this way, researchers have been studying alternatives to replace this polymer, being those belonging to the poly(2-oxazolines) family very promising. Among these, PEtOx is approved by FDA and can also improve nanoparticles' biocompatibility, blood circulation time and tumor uptake [64, 90-92].

Despite the potential of nanomaterials' mediated PDT/PTT, this approach presents some limitations. For instance, due to the oxygen deficiency in hypoxic tumors, the nanostructures' photodynamic efficacy can be greatly reduced [71, 93]. Besides that, the nanoparticles may not be able to penetrate into the tumor's core, remaining in the periphery, and as a result, their photoinduced heat will be distributed in a heterogeneous way [94].

To address these limitations, the combination of nanomaterials' PDT/PTT with other modalities, such as chemotherapy, appears to be a promising strategy. In this way, by just combining hydrophilic polymer-IR780 conjugates and a chemotherapeutic drug (*e.g.* Doxorubicin (DOX)), nanomaterials aimed for chemo-PDT/PTT can be achieved through a simple and scalable route. Such is of paramount importance since the vast majority of strategies aimed for chemo-PDT/PTT rely on the synthesis of nanomaterials with photothermal capacity (*e.g.* graphene derivatives, IR780, gold nanorods, Fe_3O_4 nanoclusters), which are subsequently loaded in their core/reservoirs with photosensitizers (*e.g.* chlorin e6, RLP068) and chemotherapeutic drugs [95-99]. Subsequently, these nanostructures still need to be coated with hydrophilic non-fouling polymers to increase their solubility and colloidal stability, and tumor-homing capacity [70, 99, 100]. Therefore, this classical strategy requires complex synthesis, assembly and functionalization steps that hinder the scale-up and translation of the nanomaterials aimed for cancer chemo-PDT/PTT.

Based on the above, the synthesis of PEtOx-IR780 conjugates, and their combination with Doxorubicin, appears to be a novel and straightforward approach for attaining nanomaterials aimed for breast cancer chemo-PDT/PTT.

1.6. Aims

The main objective of this Master Dissertation work plan was to develop a novel nanoparticle for cancer chemo-PDT/PTT with a straightforward formulation based on the use of PEtOx-IR conjugate and Doxorubicin.

The specific aims of this MSc dissertation are:

- Synthesis and characterization of a Poly(2-ethyl-2-oxazoline)-IR780 amphiphilic polymer;
- Formulation of PEtOx-IR nanoparticles (PEtOx-IR NPs) and DOX loaded PEtOx-IR nanoparticles (DOX/PEtOx-IR NPs);
- Characterization of physicochemical properties of both nanoparticles;
- Evaluation of the photodynamic and photothermal effect of PEtOx-IR NPs and DOX/PEtOx-IR NPs;
- Determination of nanomaterials' cytocompatibility in healthy and breast cancer cells;
- Evaluation of the chemo-PDT/PTT mediated by DOX/PEtOx-IR NPs towards breast cancer cells.

Chapter 2

Experimental Section

2. Experimental Section

2.1. Materials

Doxorubicin was acquired by Carbosynth (Berkshire, UK). IR780 Iodide, Poly(2-ethyl-2-oxazoline) α-benzyl ω-thiol terminated (PEtOx-SH; Mn = 10000 Da), Trypsin, Resazurin, Phosphate Buffered Saline (PBS) and Dulbecco's Modified Eagle's Medium-F12 (DMEM-F12), were bought from Sigma-Aldrich (Sintra, Portugal). Acetone, Chloroform and Methanol were attained from Fisher Scientific (Oeiras, Portugal). Triethylamine was acquired from TCI (Oxford, UK). T-flasks, Cell Culture Plates, Calcein-AM and Propidium Iodide (PI) were obtained from Thermo Fisher Scientific (Porto, Portugal). Normal Human Dermal Fibroblast (NHDF) and Michigan Cancer Foundation-7 (MCF-7) cell lines were achieved from Promocell (Heidelberg, Germany) and from ATCC (Middlesex, UK), respectively. Fetal Bovine Serum (FBS) was purchased from Biochrom AG (Berlin, Germany). Singlet Oxygen Sensor Green (SOSG) was acquired from Thermo Fisher Scientific (Porto, Portugal). Cell Imaging Plates were bought from Ibidi GmnH (Munich, Germany). Double Deionized water (0.22 μm filtered, 18.2 M Ω cm) was used in all the assays.

2.2. Methods

2.2.1. Synthesis and Characterization of PEtOx-IR Conjugate

The PEtOx-IR780 (PEtOx-IR) conjugate was synthesized by adapting previously published protocols [87, 101]. In brief, PEtOx-SH was dissolved in chloroform, followed by the addition of triethylamine and an excess of IR780. After that, the reaction was carried out for 48 h at room temperature under stirring. Subsequently, the solvent was evaporated (Rotavap® R-215, Büchi, Switzerland) and the resulting product was resuspended in methanol. Afterwards, to remove the non-conjugated IR780, a dialysis against methanol was conducted (1 kDa molecular weight cut-off membrane) for 24 h at room temperature, culminating in the obtention of the PEtOx-IR conjugate. Fourier Transform Infrared Spectroscopy (FTIR; Nicolet iS10 spectrometer, Thermo Scientific Inc., MA, USA) was used to confirm the successful synthesis of PEtOx-IR conjugate.

2.2.2. Formulation and Characterization of DOX/PEtOx-IR NPs and PEtOx-IR NPs

The production of DOX/PEtOx-IR NPs was based on the nanoprecipitation technique previously reported by Alves *et al.* [69]. Initially, DOX and PEtOx-IR conjugate dissolved in methanol:acetone (2:3 (v/v)) were added dropwise into PBS, during 2 h, with uninterrupted stirring, at room temperature. After this step, the solution was dialyzed against water (0.5 – 1 kDa molecular weight cut-off membrane) during 90 min. Then, the recovered solution was centrifuged (17 460 *g*, 1 min), being the supernatant collected which contained the DOX/PEtOx-IR NPs. For the formulation of PEtOx-IR NPs, the same procedure was used without the addition of DOX.

The size distribution (in water) and the surface charge (in DMEM-F12 medium supplemented with 10 % (v/v) FBS) of DOX/PEtOx-IR NPs and PEtOx-IR NPs were evaluated in a Zetasizer Nano ZS (Malvern Instruments Ltd., Worcestershire, UK). Absorption spectroscopy (Evolution 201 spectrophotometer, Thermo Scientific Inc.) was used to determine the Encapsulation Efficiency of DOX in DOX/PEtOx-IR NPs. For such, the DOX/PEtOx-IR NPs were freeze-dried (in a ScanVac CoolSafe, LaboGene ApS, Lynge, Denmark) and resuspended in water:methanol (1:1 (v/v)). Then, the concentration of DOX was determined by verifying the samples' absorption at 498 nm and by using a standard curve of DOX (in water:methanol (1:1 (v/v)), at 498 nm; the PEtOx-IR conjugate does not have absorbance at this wavelength in this solvent mixture). Subsequently, the Encapsulation Efficiency was calculated using the following equation (1):

$$Encapsulation\ Efficiency\ (\%) = \frac{DOX\ weight\ incorpored\ in\ the\ nanoparticles}{DOX\ weight\ initially\ fed} \times 100 \qquad (1)$$

Absorption spectroscopy was also employed to assess the ability of DOX/PEtOx-IR NPs and PEtOx-IR NPs to interact with NIR light. In this case, the absorption spectra of DOX/PEtOx-IR NPs and PEtOx-IR NPs (2.5 μg mL^{-1} of PEtOx-IR equivalents) in water were acquired.

2.2.3. Photodynamic and Photothermal effect of DOX/PEtOx-IR NPs and PEtOx-IR NPs

The photodynamic and photothermal capabilities of the nanoformulations were characterized according to literature protocols [69, 102, 103]. To evaluate the photodynamic

effect of DOX/PEtOx-IR NPs and PEtOx-IR NPs, the nanoformulations (at 2.5 μg mL^{-1} of PEtOx-IR) were mixed with SOSG (20 μL at 50 μM) and then were irradiated with NIR light (808 nm, 1.7 W cm^{-2}) during 5 min [102]. Then, the fluorescence of oxidized SOSG (λ_{ex} = 504 nm; λ_{em} = 530 nm) was measured in a spectrofluorometer (Spectramax Gemini EM spectrofluorometer, Molecular Devices LLC, CA, USA). Water (without nanoparticles) mixed with SOSG and exposed to NIR light was used as the control.

On the other hand, to verify the photothermal capacity of DOX/PEtOx-IR NPs and PEtOx-IR NPs, these nanoformulations (at 1.25 and 2.5 μg mL^{-1} of PEtOx-IR equivalents) were exposed to NIR laser irradiation (808 nm, 1.7 W cm^{-2}) during 5 min [104]. The temperature variations were measured by using a thermocouple thermometer. In this assay, the temperature variation of irradiated water (without nanoparticles) was used as control.

The procedure to evaluate the release of DOX from DOX/PEtOx-IR NPs was conducted as previously described by Alves *et al.* [104]. For such, DOX/PEtOx-IR NPs in PBS (pH 7.4) were inserted in a membrane (0.5 – 1 kDa molecular weight cut-off) and dialyzed against PBS (pH 7.4) at 37 °C under constant stirring. At predetermined time points, samples were collected and analyzed by absorption spectroscopy to determine the DOX released. DOX/PEtOx-IR NPs were also exposed to NIR light at 4 h (808 nm, 1.7 W cm^{-2}, 5 min) to verify the influence of laser irradiation on DOX release.

2.2.4. Cytocompatibility Evaluation of PEtOx-IR NPs

The cytocompatibility of PEtOx-IR NPs was evaluated in NHDF (normal cell line) and MCF-7 cells (breast cancer cell line) using the resazurin assay [63]. Initially, both cell lines (NHDF and MCF-7) were seeded (1×10^4 cells/well) in 96-wells plates with DMEM-F12 medium supplemented with 10 % (v/v) FBS and 1 % (v/v) streptomycin/gentamycin, and then placed in a humidified incubator (37 °C, 5 % CO_2). After 24 h, the medium was removed, and cells were incubated with PEtOx-IR NPs (at 1.25 and 2.5 μg mL^{-1} of PEtOx-IR equivalents) in fresh culture medium for 24 h or 48 h. Afterwards, the PEtOx-IR NPs were removed and resazurin in fresh culture medium (10 % (v/v)) was added to the cells, followed by 4 h of incubation in the dark (37 °C, 5 % CO_2). To verify the cells' viability, the resorufin fluorescence was measured in a spectrofluorometer (λ_{ex} = 560 nm; λ_{em} = 590 nm). Negative (K^-) and positive (K^+) controls were also performed using cells incubated only with fresh culture medium and with ethanol (70 % (v/v)), respectively.

2.2.5. Phototherapeutic Effect of PEtOx-IR NPs and DOX/PEtOx-IR NPs towards MCF-7 cells

The phototherapeutic effect prompted by DOX/PEtOx-IR NPs and PEtOx-IR NPs towards breast cancer cells was evaluated through the resazurin assay [105]. Firstly, MCF-7 cells were seeded as indicated in Section 2.2.4. After one day, the medium was removed, and cells were incubated with DOX/PEtOx-IR NPs (at 1.88/1.25 and 3.76/2.5 μg mL^{-1} of DOX/PEtOx-IR conjugate equivalents) or PEtOx-IR NPs (at 1.25 and 2.5 μg mL^{-1} of PEtOx-IR conjugate equivalents) in fresh culture medium. After 4 h of incubation, the cells were irradiated with NIR light (808 nm, 1.7 W cm^{-2}, 5 min). After completing 24 h of incubation with the nanoformulations, the MCF-7 cells' viability was evaluated as mentioned in Section 2.2.4.

Confocal Laser Scanning Microscopy (CLSM; Zeiss LSM confocal microscope, Carl Zeiss AG, Oberkochen, Germany) was also used to visualize the phototherapeutic effect of both nanoformulations [104]. For such, MCF-7 cells were seeded (1.5×10^4 cells/well) in μ-slide 8 well imaging plates (Ibidi GmbH, Munich, Germany). After 48 h, MCF-7 cells were incubated with fresh medium containing DOX/PEtOx-IR NPs (3.76/2.5 μg mL^{-1} of DOX/PEtOx-IR conjugate equivalents) and PEtOx-IR NPs (2.5 μg mL^{-1} of PEtOx-IR conjugate equivalents). After 4 h of incubation, cells were irradiated with NIR light (808 nm, 1.7 W cm^{-2}, 5 min). Succeeding that, the medium was removed, and cells were stained with Calcein-AM/PI to label live/dead cells, according to the manufacturer's protocol. A $\lambda_{ex}/\lambda_{em}$ of 488/493-556 nm and 561/566-719 were used to visualize Calcein-AM and PI, respectively. MCF-7 cells just incubated with culture medium (without nanoparticles/NIR light) were used as the control for live cells.

2.2.6. Statistical Analysis

To compare the different groups, a one-way Analysis of Variance (ANOVA) was applied with the Student-Newman-Keuls test. A value of p lower than 0.05 ($p < 0.05$) was considered statistically significant. To perform the data analysis, GraphPad Prism v7.0 (Trial version, GraphPad Software, CA, USA) was used.

Chapter 3

Results and Discussion

3. Results and Discussion

3.1. Synthesis and Characterization of PEtOx-IR Conjugate

PEtOx-IR conjugate was initially synthesized through the binding of PEtOx-SH to the cyclohexenyl ring of IR780. After that, the FTIR spectra of IR780, PEtOx-SH and PEtOx-IR conjugate were acquired and analyzed (Figure 7). The spectrum of IR780 showed the benzene ring stretch at 1550 cm^{-1} and the C-H bending at 757 cm^{-1} (Figure 7). On the other hand, the PEtOx-SH spectrum presented a peak at 1630 cm^{-1} that belongs to the amides' C=O stretch (Figure 7). In turn, the spectrum of PEtOx-IR conjugate presented the characteristic peaks of IR780 and PEtOx-SH, hence confirming its successful synthesis.

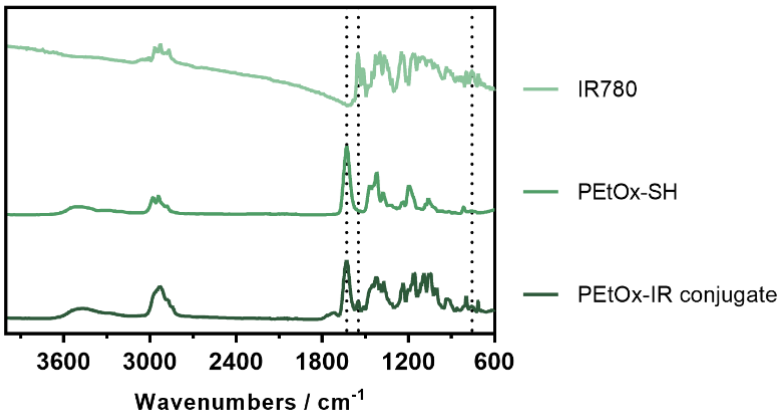

Figure 7. FTIR spectra of IR780, PEtOx-SH and PEtOx-IR conjugate.

3.2. Formulation and Characterization of DOX/PEtOx-IR NPs and PEtOx-IR NPs

After the successful synthesis of the PEtOx-IR conjugate, this polymer and DOX were used to formulate nanoparticles through the nanoprecipitation technique (termed as DOX/PEtOx-IR NPs) – Figure 8. This two-step approach was also applied to produce nanoparticles without DOX for comparison purposes (PEtOx-IR NPs).

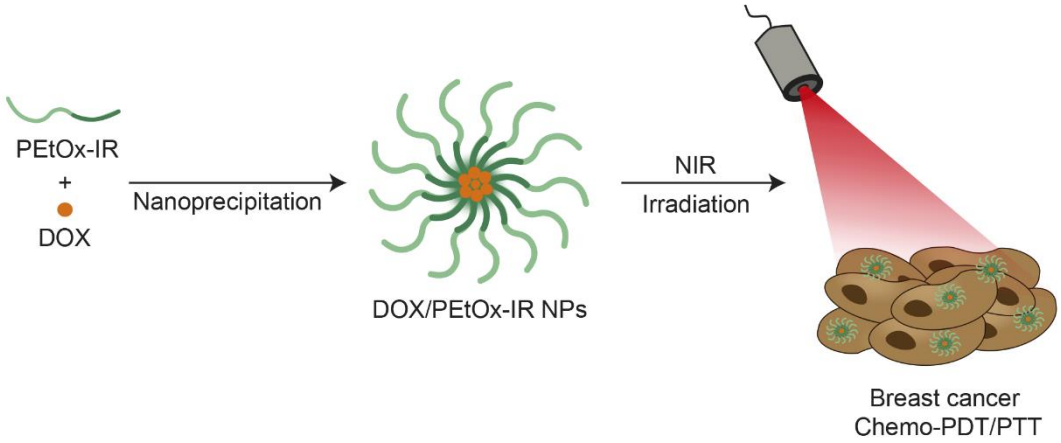

Figure 8. Schematic illustration of DOX/PEtOx-IR NPs application in cancer chemo-PDT/PTT.

Then, the nanoparticles' size was characterized by Dynamic Light Scattering (DLS) (Figure 9). PEtOx-IR NPs revealed an average size of 196.0 ± 0.5 nm and a polydispersity index (PDI) of 0.178 ± 0.005 (n = 3; batch triplicates; Figure 9). Despite their average size, the PEtOx-IR NPs displayed a small population with a size of approximately 5038 nm, indicating that these nanostructures interact with each other or that present micro-sized aggregates. Interestingly, through the encapsulation of DOX, the nanostructures' size distribution was greatly improved (Figure 9). In fact, the DOX/PEtOx-IR NPs presented an average size of 160.7 ± 3.6 nm and a PDI of 0.125 ± 0.007 (n = 3; batch triplicates; Figure 9). The DOX/PEtOx-IR NPs showed not only a smaller size but also a unique size distribution without aggregates. Such behavior could be attributed to greater hydrophobic interactions occurring between IR780 (present in the PEtOx-IR conjugate) and DOX in the core of DOX/PEtOx-IR NPs, which improved the size distribution of this formulation when compared to PEtOx-IR NPs (formulation without DOX) [106]. The DOX/PEtOx-IR NPs' size distribution is also within the range (100 – 200 nm) considered to be optimal for passive targeting to the tumor zone through the EPR effect [60].

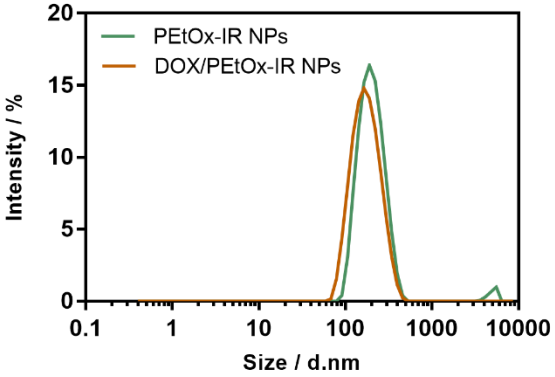

Figure 9. DLS size distribution of PEtOx-IR NPs and DOX/PEtOx-IR NPs.

The nanoparticles zeta potential was also measured, being - 8.7 ± 1.6 mV and - 9.1 ± 0.3 mV for PEtOx-IR NPs and DOX/PEtOx-IR NPs, respectively. In this regard, both formulations presented a surface charge within the optimal range for application in cancer therapy (– 10 mV to + 10 mV), which is consistent with what has been previously reported for PEtOx-coated nanomaterials [107, 108].

The DOX/PEtOx-IR NPs could also successfully encapsulate DOX with an efficiency of about 63 ± 4 %. For instance, Alves *et al.* and Deng *et al.* produced nanoparticles encapsulating DOX that presented an encapsulation efficiency of about 20 % and 14 %, respectively [104, 109]. The DOX/PEtOx-IR presented a higher DOX encapsulation efficiency, further confirming the importance of the hydrophobic interactions occurring between DOX and the PEtOx-IR conjugate in the nanoparticles' properties [104].

Then, the NIR absorption of PEtOx-IR NPs and DOX/PEtOx-IR NPs (2.5 μg mL^{-1} of PEtOx-IR conjugate) was evaluated (Figure 10A). In this regard, PEtOx-IR NPs and DOX/PEtOx-IR NPs presented absorption peaks at 791 and 792 nm, respectively (Figure 10A). As control, the absorption of the PEtOx-IR conjugate (dissolved in water:methanol (1:1 (v/v))) was also analyzed, revealing a maximum absorption peak at 781 nm (Figure 10B). Due to this red-shift in the PEtOx-IR absorption when assembled in nanostructures, the PEtOx-IR NPs and DOX/PEtOx-IR NPs showed approximately 2.4-times higher absorption at 808 nm than the PEtOx-IR conjugate. This behavior could be correlated with the hydrophobic interactions occurring in the nanoparticles' core and/or with changes in the solvents' polarity [104, 106]. The enhanced absorption at 808 nm displayed by PEtOx-IR NPs and DOX/PEtOx-IR NPs is of utmost importance since 808 nm laser light will be employed in the photodynamic/photothermal experiments, opening a venue for improved effects.

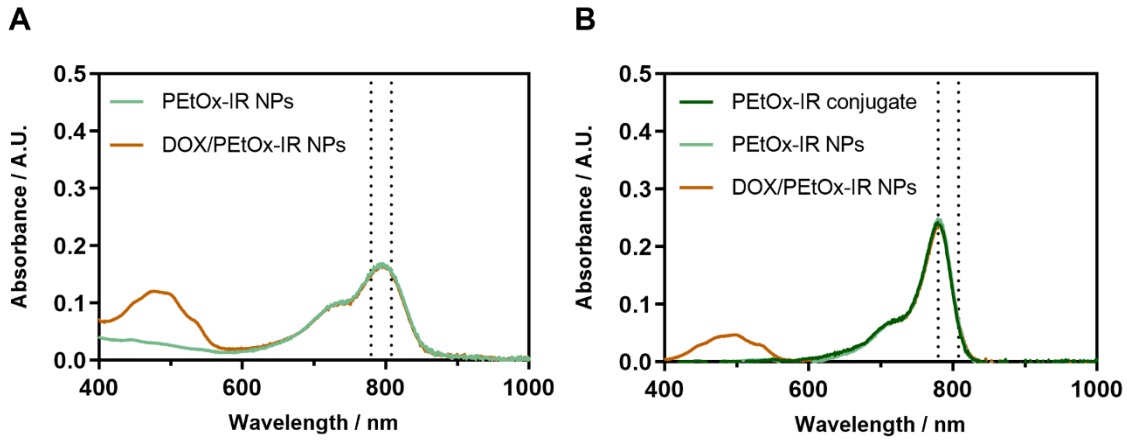

Figure 10. Absorption spectra of PEtOx-IR NPs and DOX/PEtOx-IR NPs (at 2.5 μg mL^{-1} of PEtOx-IR conjugate equivalents) in water (A). Absorption spectra of freeze-dried PEtOx-IR conjugate, PEtOx-IR NPs and DOX/PEtOx-IR NPs resuspended in water:methanol (1:1 (v/v)); at 2.5 μg mL^{-1} of PEtOx-IR conjugate equivalents (B). The dashed lines mark the wavelengths of 780 and 808 nm.

3.3. Photodynamic and Photothermal effects of DOX/PEtOx-IR NPs and PEtOx-IR NPs and NIR-enhanced DOX Release

After confirming the NIR absorption of PEtOx-IR NPs and DOX/PEtOx-IR NPs, their photodynamic and photothermal capabilities were evaluated. Initially, the photodynamic effect mediated by both formulations was investigated by using SOSG (Figure 11A and 11B). For such, the PEtOx-IR NPs and DOX/PEtOx-IR NPs with SOSG were irradiated with NIR light (808 nm, 1.7 W cm^{-2}, 5 min), and then the fluorescence of oxidized SOSG was evaluated (SOSG becomes oxidized in the presence of singlet oxygen, being this change proportional to its fluorescence levels).

In this regard, the fluorescence of oxidized SOSG rose to 866 and 901 a.u. upon interaction with PEtOx-IR NPs plus NIR light and DOX/PEtOx-IR NPs plus NIR light, respectively (both at 2.5 μg mL^{-1} of PEtOx-IR conjugate equivalents) - Figure 11A and 11B. In stark contrast, the fluorescence levels of oxidized SOSG attained for water exposed to NIR light (control) were about 2.3 – 2.4 times inferior (Figure 11A and 11B). In fact, the ability of IR780 loaded nanomaterials to produce singlet oxygen upon NIR laser irradiation was previously demonstrated in some works [103, 110]. Herein, the PEtOx-IR NPs and DOX/PEtOx-IR NPs, which are assembled using a novel PEtOx-IR conjugate, also showed ability to produce singlet oxygen upon NIR laser exposure, hence confirming their photodynamic potential.

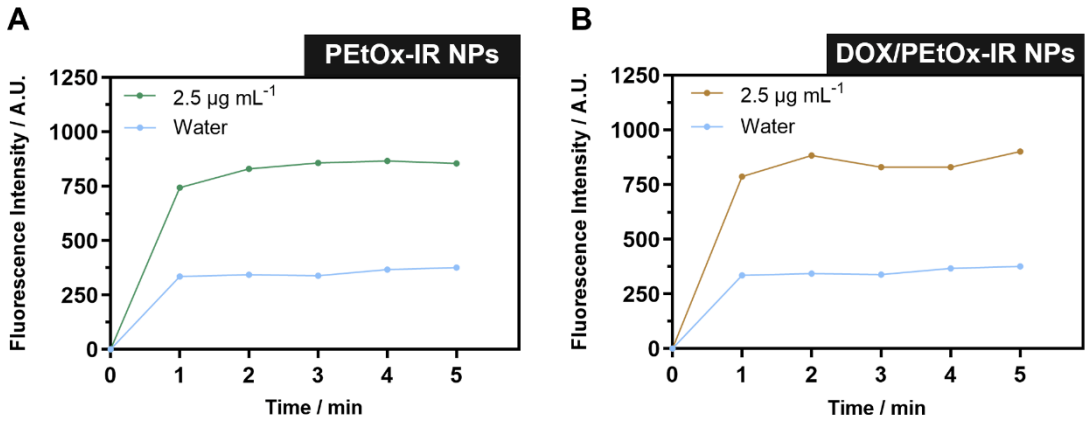

Figure 11. Photodynamic effect of PEtOx-IR NPs and DOX/PEtOx-IR NPs (at 2.5 µg mL^{-1} of PEtOx-IR conjugate equivalents). Fluorescence intensity of oxidized SOSG after interaction with PEtOx-IR NPs (A) and DOX/PEtOx-IR NPs (B) in conjugation with NIR light (808 nm, 1.7 W cm^{-2}).

To evaluate the photothermal capacity of PEtOx-IR NPs and DOX/PEtOx-IR NPs, these were irradiated with NIR light (808 nm, 1.7 W cm^{-2}, 5 min) and the temperature variations were monitored (Figure 12A and 12B). For instance, at the highest concentration tested (2.5 µg mL^{-1} of PEtOx-IR conjugate equivalents), the PEtOx-IR NPs and DOX/PEtOx-IR NPs generated, after 3 min of NIR laser irradiation, maximum temperature increases (ΔT) of 2.6 °C and 2.5 °C, respectively (Figure 12A and 12B). After this timepoint, the attained photoinduced heat started to decrease. This behavior is likely to be correlated with the photodegradation of the PEtOx-IR conjugate present on the produced nanostructures since such phenomenon has been widely reported for IR780 loaded nanostructures [104, 111]. On the other hand, water exposed to NIR light suffered a temperature increase of 1.2 °C and 1.5 °C after 3 and 5 min of NIR laser irradiation (Figure 12A and 12B). Although the PEtOx-IR NPs and DOX/PEtOx-IR NPs could produce a higher photoinduced heat than the control, their photothermal capacity was not very high, highlighting that the photodynamic pathway is likely the dominant mechanism.

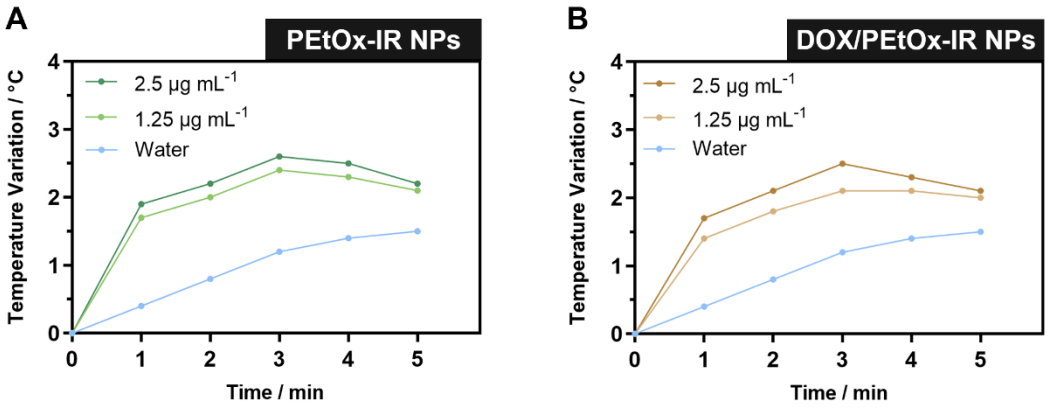

Figure 12. Photothermal effect of PEtOx-IR NPs and DOX/PEtOx-IR NPs (at different concentrations of PEtOx-IR conjugate equivalents). Temperature variation mediated by PEtOx-IR NPs (A) and DOX/PEtOx-IR NPs (B) upon exposure to NIR light (808 nm, 1.7 W cm^{-2}).

Nevertheless, the heat induced by the nanostructures could influence the release of DOX from the DOX/PEtOx-IR NPs. For such, the cumulative release of DOX from DOX/PEtOx-IR NPs was investigated in the absence and presence of NIR light (Figure 13). After the NIR laser exposure (at 4 h), the release of DOX from the DOX/PEtOx-IR NPs greatly increased (Figure 13). For instance, at the endpoint of the study, the non-irradiated nanoformulations had a 45 % DOX release, that was in plateau, while those exposed to NIR light released continuously 73 % of their cargo (Figure 13). In this way, the NIR-laser exposure could increase the release of DOX from the DOX/PEtOx-IR NPs by up to 1.6-fold (Figure 13). Altogether, these results confirm the good NIR-responsiveness of the developed formulations.

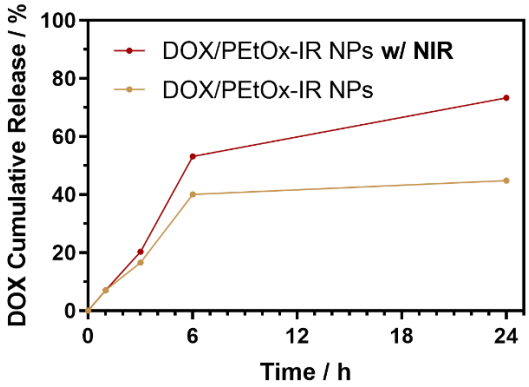

Figure 13. Cumulative release of DOX from DOX/PEtOx-IR NPs in the absence and presence of NIR light (w/ NIR; 808 nm, 1.7 W cm^{-2}, 5 min).

3.4. Cytocompatibility of PEtOx-IR NPs

In order to verify the cytocompatibility profile of the PEtOx-IR NPs, these nanostructures were incubated in NHDF and MCF-7 cells, which were used as models of healthy and breast cancer cells, respectively (Figure 14). NHDF exposed to PEtOx-IR NPs for 24 h and 48 h revealed a cell viability greater than 87 %, even at the highest concentration tested (2.5 μg mL^{-1} of PEtOx-IR conjugate equivalents) – Figure 14A. In turn, MCF-7 cells exposed to PEtOx-IR NPs demonstrated a slight reduction on their viability over time (Figure 14B). In this regard, MCF-7 cells remained with a viability of 79 % after an incubation period of 24 h with this formulation (at 2.5 μg mL^{-1} of PEtOx-IR conjugate equivalents) – Figure 14B. An incubation period of 48 h decreased slightly the MCF-7 cells' viability to about 70 % (Figure 14B). This differential effect of PEtOx-IR NPs in NHDF and MCF-7 cells can be explained by the IR780 inherent cytotoxicity towards cancer cells due to its accumulation in their mitochondria [112, 113]. In fact, this behavior has also been observed in other research works that used IR780 loaded nanomaterials for cancer therapy [69, 112, 114]. Nevertheless, the data obtained in NHDF is indicative that PEtOx-IR NPs display a good cytocompatibility towards healthy cells.

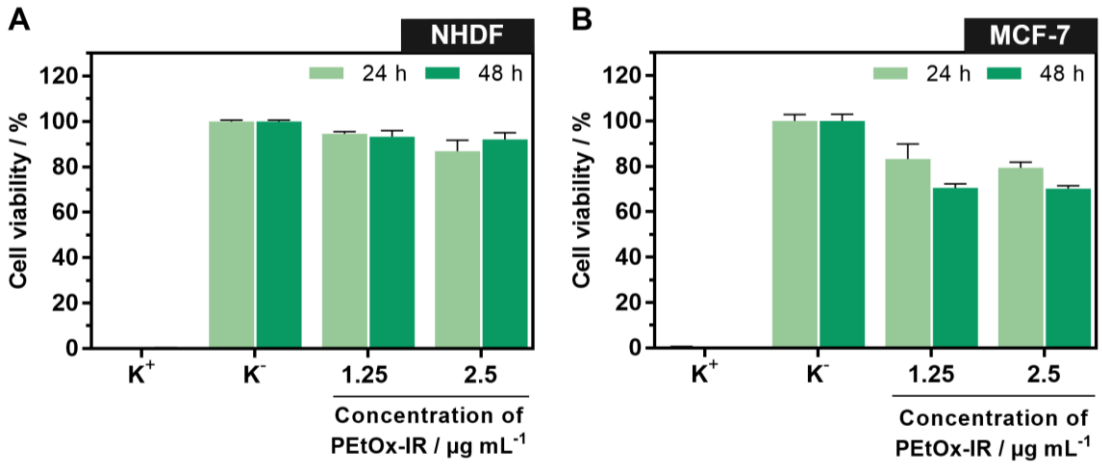

Figure 14. Determination of PEtOx-IR NPs cytocompatibility. Viability of NHDF (A) and MCF-7 cells (B) after incubation with PEtOx-IR NPs (at 1.25 and 2.5 μg mL^{-1} of PEtOx-IR conjugate equivalents) for 24 and 48 h. K^+ and K^- represent the positive and negative controls, respectively. Each bar represents the mean ± S.D. (n =5).

3.5. Phototherapeutic Effect of DOX/PEtOx-IR NPs and PEtOx-IR NPs towards MCF-7 cells

Finally, the phototherapeutic effect of both nanoparticles was evaluated in MCF-7 cells. For such, the breast cancer cells were incubated with PEtOx-IR NPs and DOX/PEtOx-IR NPs, being after 4 h exposed to NIR light (808 nm, 1.7 W cm^{-2}, 5 min) – Figure 15A. At the concentration of 1.25 μg mL^{-1} (of PEtOx-IR conjugate equivalents), the PEtOx-IR NPs did not affect meaningfully the MCF-7 cells (viability > 83 %), while PEtOx-IR NPs combined with NIR light could reduce the cells' viability to about 55 % (Figure 15B). MCF-7 cells incubated with a greater concentration of PEtOx-IR NPs (2.5 μg mL^{-1} of PEtOx-IR conjugate equivalents) also revealed a high viability (> 79 %) - Figure 15B. However, this dose of PEtOx-IR NPs combined with NIR light reduced the MCF-7 cells' viability to just 21 % (Figure 15B). As importantly, the MCF-7 cells only exposed to NIR light did not reveal any signs of nefarious effects (viability ≈ 100 %) - Figure 15B. Taken together, these results demonstrate that the on-demand outcome achieved by PEtOx-IR NPs combined with NIR light is related to the nanostructures' photodynamic/photothermal capabilities (Figure 11A and 12A).

On the other hand, the DOX/PEtOx-IR NPs reduced the viability of the MCF-7 cells to 68 % and 17 % at the concentrations of 1.88/1.25 μg mL^{-1} and 3.76/2.5 μg mL^{-1} of DOX/PEtOx-IR conjugate equivalents, respectively (Figure 15B). Since the PEtOx-IR NPs (without NIR light) barely influenced the viability of the breast cancer cells, this therapeutic outcome mediated by the DOX/PEtOx-IR NPs (without NIR light) can be attributed to the chemotherapeutic action of DOX. Interestingly, the combined action of DOX/PEtOx-IR NPs and NIR light could reduce the viability of the cancer cells to just 29 %, at an ultra-low dose of 1.88/1.25 μg mL^{-1} of DOX/PEtOx-IR conjugate equivalents (Figure 15B). The total ablation of the breast cancer cells (viability ≈ 4 %) was achieved by using a higher dose of this nanoformulation (3.76/2.5 μg mL^{-1} of DOX/PEtOx-IR conjugate equivalents) combined with NIR light, indicating the superior therapeutic efficacy of the chemo-PDT/PTT mediated by the DOX/PEtOx-IR NPs.

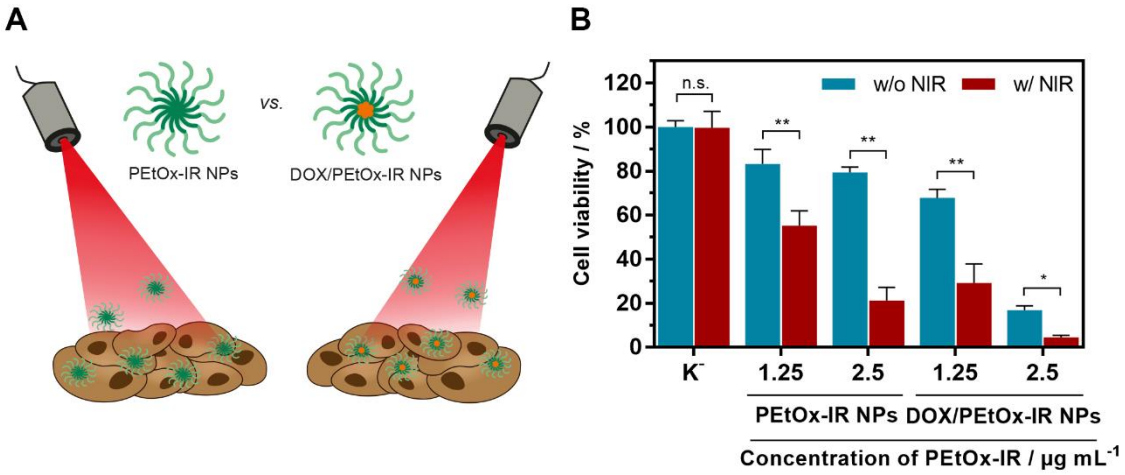

Figure 15. Schematic representation of the process used to evaluate the phototherapeutic impact of PEtOx-IR NPs and DOX/PEtOx-IR NPs on MCF-7 cells (A). Cell viability of MCF-7 cells after incubation with PEtOx-IR NPs (at 1.25 and 2.5 μg mL^{-1} of PEtOx-IR conjugate equivalents) and DOX/PEtOx-IR NPs (at 1.88/1.25 and 3.76/2.5 μg mL^{-1} of DOX/PEtOx-IR conjugate equivalents) without NIR light (w/o NIR) and with NIR light exposure (w/ NIR; 808 nm, 1.7 W cm^{-2}, 5 min) (B). K^- w/o NIR represents the negative control, and K^- w/ NIR corresponds to MCF-7 cells solely irradiated with NIR light. Data represents mean ± S.D. n = 5 (*$p < 0.01$, **$p < 0.0001$), n.s. = non-significant.

To confirm these results, the MCF-7 cells exposed to the different treatments were also stained with Calcein-AM (labels live cells) and PI (labels dead cells), being then imaged by CLSM (Figure 16A and 16B). In concomitance with the cell viability results, only Calcein-AM fluorescence signals were detected for breast cancer cells just exposed to NIR light (Figure 16B). The majority of the cancer cells incubated with PEtOx-IR NPs also displayed fluorescence from Calcein-AM (Figure 16A). In turn, Calcein-AM and PI-stained cancer cells were imaged on the groups incubated with DOX/PEtOx-IR NPs and PEtOx-IR NPs plus NIR light (Figure 15A and 15B). In contrast, only PI fluorescence signals were observed on the cancer cells exposed to DOX/PEtOx-IR NPs plus NIR light (Figure 16B), which confirms the ablative capacity arising from the nanostructures' chemo-PDT/PTT.

Xu *et al.* synthesized gold nanorods (photothermal agent; 20 μg mL^{-1}), that were coated with PEG and loaded with a protoporphyrin IX derivative (photodynamic agent; 3.20 μg mL^{-1}) and DOX (2.10 μg mL^{-1}), that after exposure to 808 nm (1 W cm^{-2}, 5 min) and 635 nm (0.5 W cm^{-2}, 5 min) radiations, could decrease MCF-7 cells viability to 37.4 % [115]. In another report, Wo *et al.* developed silica-coated hollow magnetic nanospheres (photothermal agent; 500 μg mL^{-1}) as well as carboxylated graphene quantum dots (photodynamic agent; 200 μg mL^{-1}), which together with DOX (300 μg mL^{-1}), were loaded into a liposome that could reduce the viability of cancer cells to approximately 15 % upon laser exposure (671 nm, 0.2 W cm^{-2}, 20 min) [116]. In this dissertation, the DOX/PEtOx-IR NPs were prepared using a straightforward route and their combination with NIR light

(3.76/2.5 μg mL^{-1} of DOX/PEtOx-IR conjugate equivalents; 808 nm, 1.7 W cm^{-2}, 5 min) could prompt the complete ablation of breast cancer cells, highlighting the simplicity and chemo-PDT/PTT potential of this nanosystem.

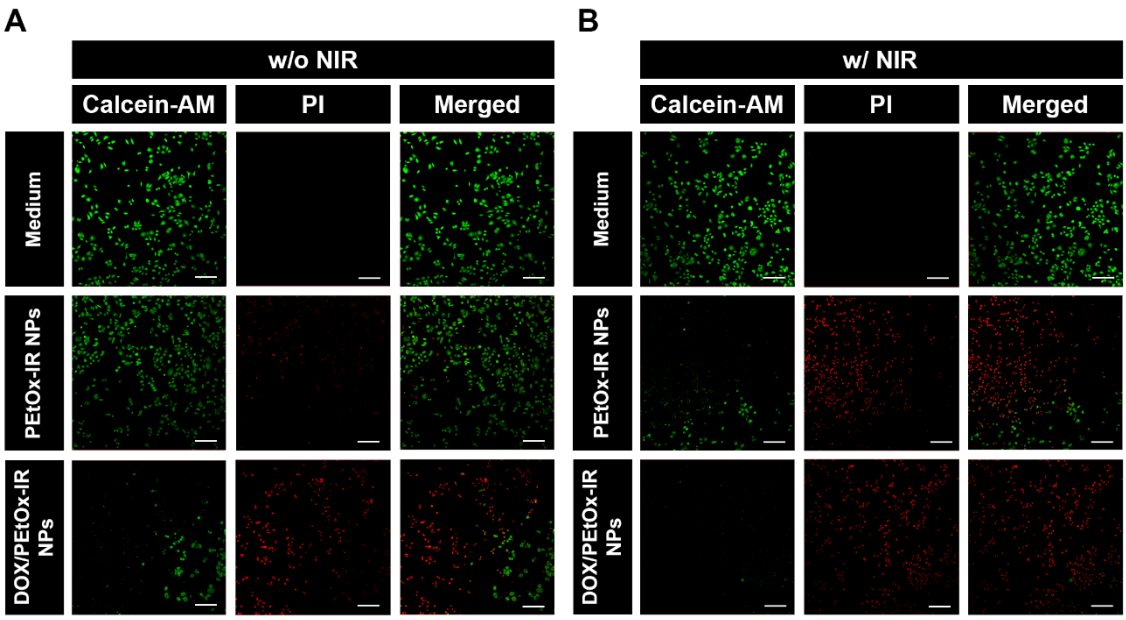

Figure 16. CLSM images of MCF-7 cells stained with Calcein-AM/PI after incubation with PEtOx-IR NPs (2.5 μg mL^{-1} of PEtOx-IR conjugate equivalents) and DOX/PEtOx-IR NPs (3.76/2.5 μg mL^{-1} of DOX/PEtOx-IR conjugate equivalents) w/o (C) and w/ NIR (D) laser irradiation (808 nm, 1.7 W cm^{-2}, 5 min). Medium w/o NIR corresponds to the control for live cells. Medium w/ NIR correspond to cells only exposed to NIR light. Green channel: Calcein-AM; Red channel: PI. Scale bars represent 200 μm.

Chapter 4

Conclusion and Future Perspectives

4. Conclusion and Future Perspectives

Despite the intense research work developed in the field of breast cancer, this disease remains as one of the deadliest among women. There are several factors that contribute to this scenario, namely the low efficacy and poor selectivity of chemo- and radio-therapies.

In order to surpass these constraints, researchers and clinicians have been focused on the development and validation of alternative approaches. Particularly, combinatorial chemo-PDT/PTT mediated by nanomaterials has been revealing promising results. This type of approach explores the intrinsic ability of nanomaterials to accumulate in the tumor zone as well as the ability of NIR light to control the onset of the therapeutic effect. As importantly, this strategy has a multimodality since it enables the ablation of cancer cells through 3 different mechanisms: ROS, heat and molecular signaling. Notwithstanding, the development of nanomaterials aimed for cancer chemo-PDT/PTT has revealed to be a complex multistep process, which impacts the potential of this technology to be scaled-up and translated into the clinical environment.

In this way, during this last year, I developed a novel and straightforward approach to attain NIR light-responsive nanosystems aimed for cancer chemo-PDT/PTT. Such was accomplished by preparing PEtOx-IR conjugates, which can be assembled into nanoparticles with photodynamic/photothermal capabilities, that simultaneously encapsulate Doxorubicin (DOX/PEtOx-IR NPs). The obtained results revealed that the DOX/PEtOx-IR NPs present a suitable size (160.7 ± 3.6 nm), dispersity (0.125 ± 0.007) and surface charge (- 9.1 ± 0.3 mV) for cancer applications. The DOX/PEtOx-IR NPs could also successfully encapsulate DOX with an efficiency of about 63 ± 4 %. Compared to the PEtOx-IR conjugate, the DOX/PEtOx-IR NPs showed about 2.4-fold higher NIR absorption (at 808 nm). Upon interaction with this radiation, the DOX/PEtOx-IR NPs produced singlet oxygen (PDT) as well as small thermic effect (PTT) that boosted the release of DOX by up to 1.6-times. In *in vitro* studies, the PEtOx-IR NPs (formulations without DOX) revealed a good cytocompatibility profile towards healthy and breast cancer cells. In turn, when the cancer cells were exposed to PEtOx-IR NPs plus NIR light (nanomaterials' PDT/PTT) and DOX/PEtOx-IR NPs (nanomaterials' chemotherapy), their viability decreased to 21 and 17 %, respectively. In contrast, the combination of DOX/PEtOx-IR NPs and NIR light led to the complete ablation of the breast cancer cells (viability < 4 %), demonstrating the enhanced therapeutic outcome arising from the nanomaterials' chemo-PDT/PTT.

In the near future, experiments using spheroids will be essential to assess more realistically the chemo-PDT/PTT effect of DOX/PEtOx-IR NPs. This characterization is crucial since

this 3D *in vitro* cancer model simulates the main features of *in vivo* solid tumors (*e.g.* 3D architecture, biochemical/physical resistance patterns and microenvironment gradients) [117, 118]. Additionally, the functionalization of the DOX/PEtOx-IR NPs with targeting ligands (*e.g.* hyaluronic acid, folic acid) may be pursued to improve the selectivity of this nano-system towards breast cancer cells. On the other hand, *in vivo* assays will also give an important insight on the DOX/PEtOx-IR NPs phototherapeutic efficiency and long-term biocompatibility. Overall, the continuous development and validation of novel chemo-PTT approaches can, in the future, contribute to reduce cancer mortality.

Chapter 5

Bibliographic References

5. Bibliographic References

[1] M.C. Hulvat, Cancer incidence and trends, Surg. Clin., 100 (2020) 469-481.

[2] H. Sung, J. Ferlay, R.L. Siegel, M. Laversanne, I. Soerjomataram, A. Jemal, F. Bray, Global cancer statistics 2020: GLOBOCAN estimates of incidence and mortality worldwide for 36 cancers in 185 countries, CA Cancer J. Clin., 71 (2021) 209-249.

[3] R.L. Siegel, K.D. Miller, H.E. Fuchs, A. Jemal, Cancer statistics, 2022, CA Cancer J. Clin., 72 (2022) 7-33.

[4] A.M. Lewandowska, M. Rudzki, S. Rudzki, T. Lewandowski, B. Laskowska, Environmental risk factors for cancer-review paper, Ann. Agric. Environ. Med., 26 (2019) 1-7.

[5] M.E. Leon, A. Peruga, A. McNeill, E. Kralikova, N. Guha, S. Minozzi, C. Espina, J. Schüz, European Code against Cancer, 4th Edition: Tobacco and cancer, Cancer Epidemiol., 39 (2015) S20-S33.

[6] J.A. Ligibel, C.M. Alfano, K.S. Courneya, W. Demark-Wahnefried, R.A. Burger, R.T. Chlebowski, C.J. Fabian, A. Gucalp, D.L. Hershman, M.M. Hudson, L.W. Jones, M. Kakarala, K.K. Ness, J.K. Merrill, D.S. Wollins, C.A. Hudis, American Society of Clinical Oncology position statement on obesity and cancer, J. Clin. Oncol., 32 (2014) 3568-3574.

[7] S.H. Hassanpour, M. Dehghani, Review of cancer from perspective of molecular, J. Cancer Res. Pract., 4 (2017) 127-129.

[8] D. Hanahan, R.A. Weinberg, Hallmarks of cancer: the next generation, Cell, 144 (2011) 646-674.

[9] R. Fior, R. Zilhão, Molecular and cell biology of cancer, Springer, 2019.

[10] D. Hanahan, Hallmarks of Cancer: New Dimensions, Cancer Discovery, 12 (2022) 31-46.

[11] A.E. Marshall, M.V. Roes, D.T. Passos, M.C. DeWeerd, A.C. Chaikovsky, J. Sage, C.J. Howlett, F.A. Dick, RB1 Deletion in Retinoblastoma Protein Pathway-Disrupted Cells Results in DNA Damage and Cancer Progression, Mol. Cell. Biol., 39 (2019) e00105-00119.

[12] E. Batlle, J. Massagué, Transforming Growth Factor-β Signaling in Immunity and Cancer, Immunity, 50 (2019) 924-940.

[13] W.A. Siddiqui, A. Ahad, H. Ahsan, The mystery of BCL2 family: Bcl-2 proteins and apoptosis: an update, Arch. Toxicol., 89 (2015) 289-317.

[14] S.M. Reed, D.E. Quelle, p53 Acetylation: Regulation and Consequences, Cancers, 7 (2015) 30-69.

[15] S.C. Akincilar, B. Unal, V. Tergaonkar, Reactivation of telomerase in cancer, Cell. Mol. Life Sci., 73 (2016) 1659-1670.

[16] Y. Xu, A. Goldkorn, Telomere and Telomerase Therapeutics in Cancer, Genes, 7 (2016) 1-21.

[17] I. Guryanov, T. Tennikova, A. Urtti, Peptide Inhibitors of Vascular Endothelial Growth Factor A: Current Situation and Perspectives, Pharmaceutics, 13 (2021) 1337.

[18] A.G. Clark, D.M. Vignjevic, Modes of cancer cell invasion and the role of the microenvironment, Curr. Opin. Cell Biol., 36 (2015) 13-22.

[19] S. Thomas, J. Izard, E. Walsh, K. Batich, P. Chongsathidkiet, G. Clarke, D.A. Sela, A.J. Muller, J.M. Mullin, K. Albert, The Host Microbiome Regulates and Maintains Human Health: A Primer and Perspective for Non-MicrobiologistsHost Microbiome in Human Health, Cancer research, 77 (2017) 1783-1812.

[20] N. Cullin, C. Azevedo Antunes, R. Straussman, C.K. Stein-Thoeringer, E. Elinav, Microbiome and cancer, Cancer Cell, 39 (2021) 1317-1341.

[21] M. Murata, Inflammation and cancer, Environ. Health Prev. Med., 23 (2018) 1-8.

[22] F.R. Greten, S.I. Grivennikov, Inflammation and Cancer: Triggers, Mechanisms, and Consequences, Immunity, 51 (2019) 27-41.

[23] D.V. Faget, Q. Ren, S.A. Stewart, Unmasking senescence: context-dependent effects of SASP in cancer, Nat. Rev. Cancer, 19 (2019) 439-453.

[24] Word Health Organizitation, Portugal Source: Globocan 2020. Acessed on 20/01/2022. Available at: https://gco.iarc.fr/today/data/factsheets/populations/620-portugal-fact-sheets.pdf.

[25] Y.-S. Sun, Z. Zhao, Z.-N. Yang, F. Xu, H.-J. Lu, Z.-Y. Zhu, W. Shi, J. Jiang, P.-P. Yao, H.-P. Zhu, Risk factors and preventions of breast cancer, Int. J. Biol. Sci., 13 (2017) 1387-1397.

[26] S.H. Giordano, Breast cancer in men, N. Engl. J. Med., 378 (2018) 2311-2320.

[27] H.R. Brewer, M.E. Jones, M.J. Schoemaker, A. Ashworth, A.J. Swerdlow, Family history and risk of breast cancer: an analysis accounting for family structure, Breast Cancer Res. Treat., 165 (2017) 193-200.

[28] K. Barzaman, J. Karami, Z. Zarei, A. Hosseinzadeh, M.H. Kazemi, S. Moradi-Kalbolandi, E. Safari, L. Farahmand, Breast cancer: Biology, biomarkers, and treatments, Int. Immunopharmacol., 84 (2020) 106535.

[29] W. Majeed, B. Aslam, I. Javed, T. Khaliq, F. Muhammad, A. Ali, A. Raza, Breast cancer: major risk factors and recent developments in treatment, Asian Pac. J. Cancer Prev., 15 (2014) 3353-3358.

[30] A. AlFakeeh, C. Brezden-Masley, Overcoming Endocrine Resistance in Hormone Receptor–Positive Breast Cancer, Curr. Oncol., 25 (2018) S18-S27.

[31] S. Farzaneh, A. Zarghi, Estrogen Receptor Ligands: A Review (2013–2015), Sci. Pharm., 84 (2016) 409-427.

[32] M.C. Louie, M.B. Sevigny, Steroid hormone receptors as prognostic markers in breast cancer, Am. J. Cancer Res., 7 (2017) 1617-1636.

[33] S. Jahan, M. Karim, E.H. Chowdhury, Nanoparticles targeting receptors on breast cancer for efficient delivery of chemotherapeutics, Biomedicines, 9 (2021) 1-30.

[34] S. Loibl, L. Gianni, HER2-positive breast cancer, The Lancet, 389 (2017) 2415-2429.

[35] M.F. Rimawi, R. Schiff, C.K. Osborne, Targeting HER2 for the treatment of breast cancer, Annual review of medicine, 66 (2015) 111-128.

[36] A.G. Waks, E.P. Winer, Breast Cancer Treatment: A Review, JAMA, 321 (2019) 288-300.

[37] P. Kumar, R. Aggarwal, An overview of triple-negative breast cancer, Arch. Gynecol. Obstet., 293 (2016) 247-269.

[38] K. Barzaman, S. Moradi-Kalbolandi, A. Hosseinzadeh, M.H. Kazemi, H. Khorramdelazad, E. Safari, L. Farahmand, Breast cancer immunotherapy: Current and novel approaches, Int. Immunopharmacol., 98 (2021) 107886.

[39] J.R. Benson, I. Jatoi, M. Keisch, F.J. Esteva, A. Makris, V.C. Jordan, Early breast cancer, The Lancet, 373 (2009) 1463-1479.

[40] E.S. McDonald, A.S. Clark, J. Tchou, P. Zhang, G.M. Freedman, Clinical diagnosis and management of breast cancer, J. Nucl. Med., 57 (2016) 9S-16S.

[41] C. Pais-Silva, D. de Melo-Diogo, I.J. Correia, IR780-loaded TPGS-TOS micelles for breast cancer photodynamic therapy, Eur. J. Pharm. Biopharm., 113 (2017) 108-117.

[42] A. Hak, V. Ravasaheb Shinde, A.K. Rengan, A review of advanced nanoformulations in phototherapy for cancer therapeutics, Photodiagn. Photodyn. Ther., 33 (2021) 102205.

[43] A.Y. Rwei, W. Wang, D.S. Kohane, Photoresponsive nanoparticles for drug delivery, Nano Today, 10 (2015) 451-467.

[44] Z. Cheng, M. Li, R. Dey, Y. Chen, Nanomaterials for cancer therapy: current progress and perspectives, J. Hematol. Oncol., 14 (2021) 2-27.

[45] Q. Zhou, L. Zhang, H. Wu, Nanomaterials for cancer therapies, Nanotechnol. Rev., 6 (2017) 473-496.

[46] D. Gao, X. Guo, X. Zhang, S. Chen, Y. Wang, T. Chen, G. Huang, Y. Gao, Z. Tian, Z. Yang, Multifunctional phototheranostic nanomedicine for cancer imaging and treatment, Mater. Today Bio, 5 (2020) 100035.

[47] T.M. Allen, P.R. Cullis, Liposomal drug delivery systems: From concept to clinical applications, Adv. Drug Delivery Rev., 65 (2013) 36-48.

[48] L. Sercombe, T. Veerati, F. Moheimani, S.Y. Wu, A.K. Sood, S. Hua, Advances and challenges of liposome assisted drug delivery, Front. Pharmacol., 6 (2015) 1-13.

[49] P. Kesharwani, K. Jain, N.K. Jain, Dendrimer as nanocarrier for drug delivery, Prog. Polym. Sci., 39 (2014) 268-307.

[50] K. Madaan, S. Kumar, N. Poonia, V. Lather, D. Pandita, Dendrimers in drug delivery and targeting: Drug-dendrimer interactions and toxicity issues, J. Pharm. BioAllied Sci., 6 (2014) 139-150.

[51] S. Movassaghian, O.M. Merkel, V.P. Torchilin, Applications of polymer micelles for imaging and drug delivery, Wiley Interdiscip. Rev.: Nanomed. Nanobiotechnol., 7 (2015) 691-707.

[52] Y. Lu, E. Zhang, J. Yang, Z. Cao, Strategies to improve micelle stability for drug delivery, Nano Res., 11 (2018) 4985-4998.

[53] S. Biswas, P. Kumari, P.M. Lakhani, B. Ghosh, Recent advances in polymeric micelles for anti-cancer drug delivery, Eur. J. Pharm. Sci., 83 (2016) 184-202.

[54] R.H. Prabhu, V.B. Patravale, M.D. Joshi, Polymeric nanoparticles for targeted treatment in oncology: current insights, Int. J. Nanomed., 10 (2015) 1001-1018.

[55] B. Li, Q. Li, J. Mo, H. Dai, Drug-loaded polymeric nanoparticles for cancer stem cell targeting, Front. Pharmacol., 8 (2017) 1-12.

[56] E. Zahmatkesh, N. Khoshdel-Rad, H. Mirzaei, A. Shpichka, P. Timashev, T. Mahmoudi, M. Vosough, Evolution of organoid technology: Lessons learnt in Co-Culture systems from developmental biology, Dev. Biol., 475 (2021) 37-53.

[57] C.F. Rodrigues, C.G. Alves, R. Lima-Sousa, A.F. Moreira, D. de Melo-Diogo, I.J. Correia, Inorganic-based drug delivery systems for cancer therapy, in: Advances and Avenues in the Development of Novel Carriers for Bioactives and Biological Agents, Elsevier, (2020) 283-316.

[58] R. Zein, W. Sharrouf, K. Selting, Physical properties of nanoparticles that result in improved cancer targeting, J. Oncol., 2020 (2020) 1-16.

[59] N. Hoshyar, S. Gray, H. Han, G. Bao, The effect of nanoparticle size on in vivo pharmacokinetics and cellular interaction, Nanomedicine, 11 (2016) 673-692.

[60] D. de Melo-Diogo, C. Pais-Silva, D.R. Dias, A.F. Moreira, I.J. Correia, Strategies to Improve Cancer Photothermal Therapy Mediated by Nanomaterials, Adv. Healthcare Mater., 6 (2017) 1700073.

[61] R. Toy, P.M. Peiris, K.B. Ghaghada, E. Karathanasis, Shaping cancer nanomedicine: the effect of particle shape on the in vivo journey of nanoparticles, Nanomedicine, 9 (2014) 121-134.

[62] A. Lesniak, A. Salvati, M.J. Santos-Martinez, M.W. Radomski, K.A. Dawson, C. Åberg, Nanoparticle Adhesion to the Cell Membrane and Its Effect on Nanoparticle Uptake Efficiency, J. Am. Chem. Soc., 135 (2013) 1438-1444.

[63] R. Lima-Sousa, D. de Melo-Diogo, C.G. Alves, E.C. Costa, P. Ferreira, R.O. Louro, I.J. Correia, Hyaluronic acid functionalized green reduced graphene oxide for targeted cancer photothermal therapy, Carbohydr. Polym., 200 (2018) 93-99.

[64] C.A. Reis, C.F. Rodrigues, A.F. Moreira, T.A. Jacinto, P. Ferreira, I.J. Correia, Development of gold-core silica shell nanospheres coated with poly-2-ethyl-oxazoline and β-cyclodextrin aimed for cancer therapy, Mater. Sci. Eng. C, 98 (2019) 960-968.

[65] D. Rosenblum, N. Joshi, W. Tao, J.M. Karp, D. Peer, Progress and challenges towards targeted delivery of cancer therapeutics, Nat. Commun., 9 (2018) 1410.

[66] Z.C. Soe, R.K. Thapa, W. Ou, M. Gautam, H.T. Nguyen, S.G. Jin, S.K. Ku, K.T. Oh, H.-G. Choi, C.S. Yong, Folate receptor-mediated celastrol and irinotecan combination delivery using liposomes for effective chemotherapy, Colloids Surf., B, 170 (2018) 718-728.

[67] J. Li, W. Xu, X. Yuan, H. Chen, H. Song, B. Wang, J. Han, Polymer-lipid hybrid anti-HER2 nanoparticles for targeted salinomycin delivery to HER2-positive breast cancer stem cells and cancer cells, Int. J. Nanomed., 12 (2017) 6909-6921.

[68] L. Wang, C. Niu, IR780-based nanomaterials for cancer imaging and therapy, J. Mater. Chem. B, 9 (2021) 4079-4097.

[69] C.G. Alves, D. de Melo-Diogo, R. Lima-Sousa, I.J. Correia, IR780 loaded sulfobetaine methacrylate-functionalized albumin nanoparticles aimed for enhanced breast cancer phototherapy, Int. J. Pharm., 582 (2020) 119346.

[70] C.G. Alves, R. Lima-Sousa, D. de Melo-Diogo, R.O. Louro, I.J. Correia, IR780 based nanomaterials for cancer imaging and photothermal, photodynamic and combinatorial therapies, Int. J. Pharm., 542 (2018) 164-175.

[71] L. Huang, S. Zhao, J. Wu, L. Yu, N. Singh, K. Yang, M. Lan, P. Wang, J.S. Kim, Photodynamic therapy for hypoxic tumors: Advances and perspectives, Coord. Chem. Rev., 438 (2021) 213888.

[72] A.S. Gonçalves, C.F. Rodrigues, A.F. Moreira, I.J. Correia, Strategies to improve the photothermal capacity of gold-based nanomedicines, Acta Biomater., 116 (2020) 105-137.

[73] H. Shi, P.J. Sadler, How promising is phototherapy for cancer?, Br. J. Cancer, 123 (2020) 871-873.

[74] Q. Ban, T. Bai, X. Duan, J. Kong, Noninvasive photothermal cancer therapy nanoplatforms via integrating nanomaterials and functional polymers, Biomater. Sci., 5 (2017) 190-210.

[75] J. Li, W. Zhang, W. Ji, J. Wang, N. Wang, W. Wu, Q. Wu, X. Hou, W. Hu, L. Li, Near Infrared Photothermal Conversion Materials: Mechanism, Preparation and Photothermal Cancer Therapy Applications, J. Mater. Chem. B, 9 (2021) 7909-7926.

[76] G. Yang, J. Liu, Y. Wu, L. Feng, Z. Liu, Near-infrared-light responsive nanoscale drug delivery systems for cancer treatment, Coord. Chem. Rev., 320-321 (2016) 100-117.

[77] H.S. Jung, P. Verwilst, A. Sharma, J. Shin, J.L. Sessler, J.S. Kim, Organic molecule-based photothermal agents: an expanding photothermal therapy universe, Chem. Soc. Rev., 47 (2018) 2280-2297.

[78] B. Liu, C. Li, Z. Cheng, Z. Hou, S. Huang, J. Lin, Functional nanomaterials for near-infrared-triggered cancer therapy, Biomater. Sci., 4 (2016) 890-909.

[79] M.M. Leitão, D. de Melo-Diogo, C.G. Alves, R. Lima-Sousa, I.J. Correia, Prototypic heptamethine cyanine incorporating nanomaterials for cancer phototheragnostic, Adv. Healthcare Mater., 9 (2020) 1901665.

[80] Y. Chen, Z. Li, H. Wang, Y. Wang, H. Han, Q. Jin, J. Ji, IR-780 Loaded Phospholipid Mimicking Homopolymeric Micelles for Near-IR Imaging and Photothermal Therapy of Pancreatic Cancer, ACS Appl. Mater. Interfaces, 8 (2016) 6852-6858.

[81] Y. Wang, L. Feng, S. Wang, Conjugated polymer nanoparticles for imaging, cell activity regulation, and therapy, Adv. Funct. Mater., 29 (2019) 1806818.

[82] T. Lin, A. Yuan, X. Zhao, H. Lian, J. Zhuang, W. Chen, Q. Zhang, G. Liu, S. Zhang, W. Chen, W. Cao, C. Zhang, J. Wu, Y. Hu, H. Guo, Self-assembled tumor-targeting hyaluronic acid nanoparticles for photothermal ablation in orthotopic bladder cancer, Acta Biomater., 53 (2017) 427-438.

[83] J. Nicolas, Drug-Initiated Synthesis of Polymer Prodrugs: Combining Simplicity and Efficacy in Drug Delivery, Chemistry of Materials, 28 (2016) 1591-1606.

[84] S. Manandhar, E. Sjöholm, J. Bobacka, J.M. Rosenholm, K.K. Bansal, Polymer-Drug Conjugates as Nanotheranostic Agents, J. Nanotheranostics, 2 (2021) 63-81.

[85] S.K. Ghosh, A. Böker, Self-Assembly of Nanoparticles in 2D and 3D: Recent Advances and Future Trends, Macromol. Chem. Phys., 220 (2019) 1900196.

[86] H. Jin, X. Lin, M. Gao, L. Cui, Y. Liu, Peptide-Decorated Supramolecules for Subcellular Targeted Cancer Therapy: Recent Advances, Front. Chem., 8 (2020) 1-7.

[87] A. Yuan, X. Qiu, X. Tang, W. Liu, J. Wu, Y. Hu, Self-assembled PEG-IR-780-C13 micelle as a targeting, safe and highly-effective photothermal agent for in vivo imaging and cancer therapy, Biomaterials, 51 (2015) 184-193.

[88] P. Zhang, F. Sun, S. Liu, S. Jiang, Anti-PEG antibodies in the clinic: Current issues and beyond PEGylation, J. Controlled Release, 244 (2016) 184-193.

[89] S. Nemati Mahand, S. Aliakbarzadeh, A. Moghaddam, A. Salehi Moghaddam, B. Kruppke, M. Nasrollahzadeh, H.A. Khonakdar, Polyoxazoline: A review article from polymerization to smart behaviors and biomedical applications, Eur. Polym. J., 178 (2022) 111484.

[90] O. Koshkina, D. Westmeier, T. Lang, C. Bantz, A. Hahlbrock, C. Würth, U. Resch-Genger, U. Braun, R. Thiermann, C. Weise, M. Eravci, B. Mohr, H. Schlaad, R.H. Stauber, D. Docter, A. Bertin, M. Maskos, Tuning the Surface of Nanoparticles: Impact of Poly(2-ethyl-2-oxazoline) on Protein Adsorption in Serum and Cellular Uptake, Macromol. Biosci., 16 (2016) 1287-1300.

[91] S. Gulyuz, D. Bayram, U.U. Ozkose, Z.B. Bolat, P. Kocak, O.M. Saka, B. Devrim, M. Parlak Khalily, D. Telci, F. Sahin, S. Özçubukçu, E. Sezer, M.A. Tasdelen, O. Alpturk, A. Bozkır, O. Yilmaz, Synthesis, biocompatibility and gene encapsulation of poly(2-Ethyl 2-Oxazoline)-dioleoyl phosphatidylethanolamine (PEtOx-DOPE) and post-modifications with peptides and fluorescent dye coumarin, Int. J. Polym. Mater. Polym. Biomater., 70 (2021) 981-993.

[92] O. Sedlacek, V.R. de la Rosa, R. Hoogenboom, Poly(2-oxazoline)-protein conjugates, Eur. Polym. J., 120 (2019) 109246.

[93] B.S. Dash, S. Das, J.-P. Chen, Photosensitizer-Functionalized Nanocomposites for Light-Activated Cancer Theranostics, Int. J. Mol. Sci., 22 (2021) 1-22.

[94] Y. Xing, T. Ding, Z. Wang, L. Wang, H. Guan, J. Tang, D. Mo, J. Zhang, Temporally controlled photothermal/photodynamic and combined therapy for overcoming multidrug

resistance of cancer by polydopamine nanoclustered micelles, ACS Appl. Mater. Interfaces, 11 (2019) 13945-13953.

[95] H. Abrahamse, Michael R. Hamblin, New photosensitizers for photodynamic therapy, Biochem. J., 473 (2016) 347-364.

[96] L. Zou, H. Wang, B. He, L. Zeng, T. Tan, H. Cao, X. He, Z. Zhang, S. Guo, Y. Li, Current approaches of photothermal therapy in treating cancer metastasis with nanotherapeutics, Theranostics, 6 (2016) 762-772.

[97] N. Fernandes, C.F. Rodrigues, A.F. Moreira, I.J. Correia, Overview of the application of inorganic nanomaterials in cancer photothermal therapy, Biomater. Sci., 8 (2020) 2990-3020.

[98] M. Lan, S. Zhao, W. Liu, C.-S. Lee, W. Zhang, P. Wang, Photosensitizers for Photodynamic Therapy, Adv. Healthcare Mater., 8 (2019) 1900132.

[99] X. Qin, Z. Wang, C. Guo, Y. Jin, Multi-responsive drug delivery nanoplatform for tumor-targeted synergistic photothermal/dynamic therapy and chemotherapy, New Journal of Chemistry, 44 (2020) 3593-3603.

[100] M.J. Mitchell, M.M. Billingsley, R.M. Haley, M.E. Wechsler, N.A. Peppas, R. Langer, Engineering precision nanoparticles for drug delivery, Nat. Rev. Drug Discovery, 20 (2021) 101-124.

[101] N. Luo, J.K. Weber, S. Wang, B. Luan, H. Yue, X. Xi, J. Du, Z. Yang, W. Wei, R. Zhou, G. Ma, PEGylated graphene oxide elicits strong immunological responses despite surface passivation, Nat. Commun., 8 (2017) 14537.

[102] C. Jiang, H. Cheng, A. Yuan, X. Tang, J. Wu, Y. Hu, Hydrophobic IR780 encapsulated in biodegradable human serum albumin nanoparticles for photothermal and photodynamic therapy, Acta Biomater, 14 (2015) 61-69.

[103] S. Ma, J. Zhou, Y. Zhang, B. Yang, Y. He, C. Tian, X. Xu, Z. Gu, An Oxygen Self-sufficient Fluorinated Nanoplatform for Relieved Tumor Hypoxia and Enhanced Photodynamic Therapy of Cancers, ACS Appl. Mater. Interfaces, 11 (2019) 7731-7742.

[104] C.G. Alves, D. de Melo-Diogo, R. Lima-Sousa, E.C. Costa, I.J. Correia, Hyaluronic acid functionalized nanoparticles loaded with IR780 and DOX for cancer chemo-photothermal therapy, Eur. J. Pharm. Biopharm., 137 (2019) 86-94.

[105] D. de Melo-Diogo, E.C. Costa, C.G. Alves, R. Lima-Sousa, P. Ferreira, R.O. Louro, I.J. Correia, POxylated graphene oxide nanomaterials for combination chemo-phototherapy of breast cancer cells, Eur. J. Pharm. Biopharm., 131 (2018) 162-169.

[106] Y. Tan, Y. Zhu, L. Wen, X. Yang, X. Liu, T. Meng, S. Dai, Y. Ping, H. Yuan, F. Hu, Mitochondria-Responsive Drug Release along with Heat Shock Mediated by Multifunctional Glycolipid Micelles for Precise Cancer Chemo-Phototherapy, Theranostics, 9 (2019) 691-707.

[107] Y. Gao, Y. Zhou, L. Zhao, C. Zhang, Y. Li, J. Li, X. Li, Y. Liu, Enhanced antitumor efficacy by cyclic RGDyK-conjugated and paclitaxel-loaded pH-responsive polymeric micelles, Acta Biomater., 23 (2015) 127-135.

[108] Z.B. Bolat, A.E. Nezir, B. Devrim, E. Zemheri, S. Gulyuz, U.U. Ozkose, O. Yilmaz, A. Bozkir, D. Telci, F. Sahin, Delivery of doxorubicin loaded P18 conjugated-poly(2-ethyl-oxazoline)-DOPE nanoliposomes for targeted therapy of breast cancer, Toxicol. Appl. Pharmacol., 428 (2021) 115671.

[109] H. Deng, X. Zhao, L. Deng, J. Liu, A. Dong, Reactive oxygen species activated nanoparticles with tumor acidity internalization for precise anticancer therapy, J. Controlled Release, 255 (2017) 142-153.

[110] D. Wang, S. Zhang, T. Zhang, G. Wan, B. Chen, Q. Xiong, J. Zhang, W. Zhang, Y. Wang, Pullulan-coated phospholipid and Pluronic F68 complex nanoparticles for carrying IR780 and paclitaxel to treat hepatocellular carcinoma by combining photothermal therapy/photodynamic therapy and chemotherapy, Int. J. Nanomed., 12 (2017) 8649-8670.

[111] G. Wan, Y. Cheng, J. Song, Q. Chen, B. Chen, Y. Liu, S. Ji, H. Chen, Y. Wang, Nucleus-targeting near-infrared nanoparticles based on TAT peptide-conjugated IR780 for photo-chemotherapy of breast cancer, Chem. Eng. J., 380 (2020) 122458.

[112] Y. Wang, T. Liu, E. Zhang, S. Luo, X. Tan, C. Shi, Preferential accumulation of the near infrared heptamethine dye IR-780 in the mitochondria of drug-resistant lung cancer cells, Biomaterials, 35 (2014) 4116-4124.

[113] R. Zhao, X. Ning, M. Wang, A. Yu, Y. Wang, A multifunctional nano-delivery system enhances the chemo-co-phototherapy of tumor multidrug resistance via mitochondrial-targeting and inhibiting P-glycoprotein-mediated efflux, J. Mater. Chem. B, 9 (2021) 9174-9182.

[114] M. Chen, N. Bhattarai, M. Cong, R.L. Pérez, K.C. McDonough, I.M. Warner, Mitochondria targeting IR780-based nanoGUMBOS for enhanced selective toxicity towards cancer cells, RSC Adv., 8 (2018) 31700-31709.

[115] W. Xu, J. Qian, G. Hou, Y. Wang, J. Wang, T. Sun, L. Ji, A. Suo, Y. Yao, PEGylated hydrazided gold nanorods for pH-triggered chemo/photodynamic/photothermal triple therapy of breast cancer, Acta Biomater., 82 (2018) 171-183.

[116] F. Wo, R. Xu, Y. Shao, Z. Zhang, M. Chu, D. Shi, S. Liu, A Multimodal System with Synergistic Effects of Magneto-Mechanical, Photothermal, Photodynamic and Chemo Therapies of Cancer in Graphene-Quantum Dot-Coated Hollow Magnetic Nanospheres, Theranostics, 6 (2016) 485-500.

[117] D. Liu, S. Chen, M. Win Naing, A review of manufacturing capabilities of cell spheroid generation technologies and future development, Biotechnol. Bioeng., 118 (2021) 542-554.

[118] A.S. Nunes, A.S. Barros, E.C. Costa, A.F. Moreira, I.J. Correia, 3D tumor spheroids as in vitro models to mimic in vivo human solid tumors resistance to therapeutic drugs, Biotechnol. Bioeng., 116 (2019) 206-226.